A&A 577, A6 (2015)
DOI: 10.1051/0004-6361/201425326

Astronomy & Astrophysics

Stellar laboratories

IV. New Ga IV, Ga V, and Ga VI oscillator strengths and the gallium abundance in the hot white dwarfs G191−B2B and RE 0503−289⋆,⋆⋆,⋆⋆⋆,⋆⋆⋆⋆

T. Rauch[1], K. Werner[1], P. Quinet[2,3], and J. W. Kruk[4]

[1] Institute for Astronomy and Astrophysics, Kepler Center for Astro and Particle Physics, Eberhard Karls University, Sand 1, 72076 Tübingen, Germany
e-mail: rauch@astro.uni-tuebingen.de
[2] Astrophysique et Spectroscopie, Université de Mons – UMONS, 7000 Mons, Belgium
[3] IPNAS, Université de Liège, Sart Tilman, 4000 Liège, Belgium
[4] NASA Goddard Space Flight Center, Greenbelt, MD 20771, USA

Received 13 November 2014 / Accepted 23 January 2015

ABSTRACT

Context. For the spectral analysis of high-resolution and high-signal-to-noise (S/N) spectra of hot stars, advanced non-local thermodynamic equilibrium (NLTE) model atmospheres are mandatory. These atmospheres are strongly dependent on the reliability of the atomic data that are used to calculate them.
Aims. Reliable Ga IV–VI oscillator strengths are used to identify Ga lines in the spectra of the DA-type white dwarf G191−B2B and the DO-type white dwarf RE 0503−289 and to determine their photospheric Ga abundances.
Methods. We newly calculated Ga IV–VI oscillator strengths to consider their radiative and collisional bound-bound transitions in detail in our NLTE stellar-atmosphere models for analyzing of Ga lines exhibited in high-resolution and high-S/N UV observations of G191−B2B and RE 0503−289.
Results. We unambiguously detected 20 isolated and 6 blended (with lines of other species) Ga V lines in the Far Ultraviolet Spectroscopic Explorer (FUSE) spectrum of RE 0503−289. The identification of Ga IV and Ga VI lines is uncertain because they are weak and partly blended by other lines. The determined Ga abundance is $3.5 \pm 0.5 \times 10^{-5}$ (mass fraction, about 625 times the solar value). The Ga IV/Ga V ionization equilibrium, which is a very sensitive indicator for the effective temperature, is well reproduced in RE 0503−289. We identified the strongest Ga IV lines (at 1258.801, 1338.129 Å) in the HST/STIS spectrum of G191−B2B and measured a Ga abundance of $2.0 \pm 0.5 \times 10^{-6}$ (about 22 times solar).
Conclusions. Reliable measurements and calculations of atomic data are a prerequisite for stellar-atmosphere modeling. The observed Ga IV–V line profiles in two white dwarf (G191−B2B and RE 0503−289) ultraviolet spectra were well reproduced with our newly calculated oscillator strengths. For the first time, this allowed us to determine the photospheric Ga abundance in white dwarfs.

Key words. atomic data – line: identification – stars: abundances – stars: individual: G191–B2B – stars: individual: RE 0503−289 – virtual observatory tools

1. Introduction

The spectral lines of ten trans-iron elements were detected by Werner et al. (2012) in the hydrogen-deficient DO-type white dwarf (WD) RE 0503−289. The authors used Far Ultraviolet Spectroscopic Explorer (FUSE) spectra with a high resolution and high signal-to-noise ratio (S/N). RE 0503−289 has an effective temperature of $T_{\rm eff}$ = 70 000 K and a surface gravity of $\log(g/{\rm cm/s^2}) = 7.5$. (Dreizler & Werner 1996). Ga and Mo were identified for the first time in a WD. An abundance analysis was performed by Werner et al. (2012) for Kr and Xe (−4.3 ± 0.5 and −4.2 ± 0.6 in logarithmic mass fractions, respectively) alone because they lacked atomic data for the other newly identified, highly ionized species.

New calculations of reliable transition probabilities (not only for the identified lines themselves, but for the complete model atom that is considered in the model atmosphere and spectral energy distribution (SED) calculations) are mandatory for precise abundance analyses. These enabled us to measure the Zn (Rauch et al. 2014a), Ge (Rauch et al. 2012), and Ba (Rauch et al. 2014b) abundances in RE 0503−289 and the hydrogen-rich DA-type WD G191−B2B ($T_{\rm eff}$ = 60 000 K, $\log g = 7.6$, Rauch et al. 2013). The Sn abundance in G191−B2B was determined based on existing atomic data (Rauch et al. 2013). Our models strongly reduced the number of unidentified lines in the spectra of RE 0503−289 and G191−B2B.

⋆ Based on observations with the NASA/ESA *Hubble* Space Telescope, obtained at the Space Telescope Science Institute, which is operated by the Association of Universities for Research in Astronomy, Inc., under NASA contract NAS5-26666.
⋆⋆ Based on observations made with the NASA-CNES-CSA Far Ultraviolet Spectroscopic Explorer.
⋆⋆⋆ Tables 1–6, 11, 12 and 15 are available in electronic form at http://www.aanda.org
⋆⋆⋆⋆ Tables 7–9 are only available at the CDS via anonymous ftp to cdsarc.u-strasbg.fr (130.79.128.5) or via http://cdsarc.u-strasbg.fr/viz-bin/qcat?J/A+A/577/A6

Since Werner et al. (2012) identified more than a dozen Ga V lines in the FUSE spectrum of RE 0503−289, we computed Ga IV–VI transition probabilities (Sect. 2) and calculated non-local thermodynamic equilibrium (NLTE) model-atmosphere spectra (Sect. 4) for an accurate Ga-abundance determination (Sect. 5). We summarize our results and conclude in Sect. 6.

2. Atomic structure and radiative data calculation

Many spectral lines of Ga IV, Ga V, and Ga VI were observed in laboratories in the past. This allowed identifying very many energy levels of Ga IV, Ga V, and Ga VI that were listed by Shirai et al. (2007), who made a critical compilation of all the experimental data previously published by Mack et al. (1928), Moore (1971), Ryabtsev (1975), Ramonas & Ryabtsev (1990), and Ryabtsev & Churilov (1991) for Ga IV, Sawyer & Humphreys (1928), Kononov (1967), Joshi et al. (1972), Aksenov & Ryabtsev (1974), Dick (1974), van Deurzen (1977), and Ryabtsev & Ramonas (1985) for Ga V, and Podobedova et al. (1983, 1985) for Ga VI.

In the present work, new sets of oscillator strengths and transition probabilities were obtained for Ga IV, Ga V, and Ga VI. These were computed using the pseudo-relativistic Hartree-Fock (HFR) approach of Cowan (1981) combined with a semi-empirical least-squares fit of radial energy parameters. In each ion, many electron correlations were considered by means of extended multiconfiguration expansions that are included in the physical models. These expansions were chosen so as to include low-lying configurations for which energy levels are experimentally known together with some higher configurations with large configuration interaction Slater integrals R^k that connect these latter configurations to the former.

More precisely, in Ga IV, configuration interaction was explicitly considered among the configurations $3d^{10}$, $3d^9 4s$, $3d^9 5s$, $3d^9 6s$, $3d^9 7s$, $3d^9 4d$, $3d^9 5d$, $3d^9 6d$, $3d^9 7d$, $3d^8 4s^2$, $3d^8 4p^2$, $3d^8 4d^2$, $3d^8 4f^2$, $3d^8 4s5s$, $3d^8 4s6s$, $3d^8 4s7s$, $3d^8 4s4d$, $3d^8 4s5d$, $3d^8 4s6d$, $3d^8 4s7d$, and $3d^8 4p4f$ for the even parity, and $3d^9 4p$, $3d^9 5p$, $3d^9 6p$, $3d^9 7p$, $3d^9 4f$, $3d^9 5f$, $3d^9 6f$, $3d^9 7f$, $3d^8 4s4p$, $3d^8 4s5p$, $3d^8 4s6p$, $3d^8 4s7p$, $3d^8 4s4f$, $3d^8 4s5f$, $3d^8 4s6f$, $3d^8 4s7f$, and $3d^8 4p4d$ for the odd parity. Using experimental energy levels reported by Shirai et al. (2007), the radial integrals (average energy, Slater, spin-orbit parameters and effective interaction parameters) of $3d^{10}$, $3d^9 4s$, $3d^9 5s$, $3d^9 6s$, $3d^9 7s$, $3d^9 4d$, $3d^9 5d$, and $3d^9 6d$ for even configurations and $3d^9 4p$, $3d^9 5p$, $3d^9 6p$, $3d^9 4f$, $3d^8 4s4p$ for odd configurations were optimized by a well-established fitting procedure. The mean deviations between computed and experimental energy levels were 61 cm^{-1} (71 levels) and 52 cm^{-1} (116 levels) for even and odd parities, respectively.

For Ga V, the HFR method was used with, as interacting configurations, $3d^9$, $3d^8 4s$, $3d^8 5s$, $3d^8 4d$, $3d^8 5d$, $3d^7 4s^2$, $3d^7 4p^2$, $3d^7 4d^2$, $3d^7 4f^2$, $3d^7 4s5s$, $3d^7 4s4d$, and $3d^7 4s5d$ for the even parity, and $3d^8 4p$, $3d^8 5p$, $3d^8 4f$, $3d^8 5f$, $3d^7 4s4p$, $3d^7 4s5p$, $3d^7 4s4f$, $3d^7 4s5f$, and $3d^7 4p4d$ for the odd parity. The radial integrals corresponding to $3d^9$, $3d^8 4s$, $3d^8 4p$, and $3d^8 4f$ were adjusted to minimize the differences between the calculated Hamiltonian eigenvalues and the experimental energy levels taken from Shirai et al. (2007). In this process, we found mean deviations equal to 34 cm^{-1} (17 levels) in the even parity and 108 cm^{-1} (74 levels) in the odd parity.

Finally, in the case of Ga VI, the configurations included in the HFR model were $3d^8$, $3d^7 4s$, $3d^7 4d$, $3d^6 4s^2$, $3d^6 4p^2$, $3d^6 4d^2$, and $3d^6 4s4d$ for the even parity, and $3d^7 4p$, $3d^7 4f$, $3d^6 4s4p$, $3d^6 4s4f$, and $3d^6 4p4d$ for the odd parity. The experimental energy levels reported by Shirai et al. (2007) were used here as well to optimize the radial integrals characterizing the $3d^8$, $3d^7 4s$, and $3d^7 4p$ configurations. This semi-empirical process led to average deviations with experimental data equal to 122 cm^{-1} (47 levels) and 161 cm^{-1} (110 levels) for even and odd parities, respectively.

The numerical values of the parameters adopted in the present calculations are reported in Tables 1–3, while the computed energies are compared with available experimental values in Tables 4–6, for Ga IV, Ga V, and Ga VI, respectively. Tables 7–9 give the HFR oscillator strengths ($\log gf$) and transition probabilities (gA, in s^{-1}) for Ga IV–VI, respectively, and the numerical values (in cm^{-1}) of lower and upper energy levels and the corresponding wavelengths (in Å). In the last column of each table, we also give the absolute value of the cancellation factor CF as defined by Cowan (1981). We note that very low values of this factor (typically <0.05) indicate strong cancellation effects in the calculation of line strengths. In these cases, the corresponding gf and gA values could be very inaccurate and therefore need to be considered with some care. However, very few of the transitions appearing in Tables 7–9 are affected.

3. Observations

We analyzed the FUSE spectrum (910 Å $< \lambda <$ 1188 Å, resolving power $R = \lambda/\Delta\lambda \approx 20\,000$) of RE 0503−289 and for G191−B2B FUSE and *Hubble* Space Telescope/Space Telescope Imaging Spectrograph spectra (HST/STIS, 1145 Å $< \lambda <$ 1750 Å). The latter is co-added from 105 observations with the highest resolution[1]. These spectra were previously described in detail by Werner et al. (2012) and Rauch et al. (2013), respectively.

In addition, we used our recently obtained (and later co-added) HST/STIS spectra of RE 0503−289 (2014-08-14, ObsIds OC7N01010, OC7N01020, grating E140M, $R \approx 45\,800$, total exposure time 5494 s).

All spectra are available via the Barbara A. Mikulski Archive for Space Telescopes (MAST[2]).

4. Model atmospheres and atomic data

The Tübingen NLTE model-atmosphere package (TMAP[3], Werner et al. 2003; Rauch & Deetjen 2003) was used to calculate advanced plane-parallel and chemically homogeneous stellar model atmospheres in radiative and hydrostatic equilibrium.

In our recent abundance analyses of trans-iron elements (Rauch et al. 2014a,b), we encountered the problem that with a new species included in the models, our model-atmosphere code would not compile if the array sizes were increased to account for the higher number of atomic levels treated in NLTE and the respective higher number of radiative and collisional transitions. Therefore, we decided at that time to reduce the number of levels of various species in our model atoms that were treated in NLTE. This did not have a significant effect on the abundance analyses. However, since we plan to continue the abundance analyses of trans-iron elements, an incalculable, systematic error may arise.

[1] Grating E140H, $R \approx 118\,000$, http://www.stsci.edu/hst/observatory/crds/calspec.html
[2] http://archive.stsci.edu/
[3] http://astro.uni-tuebingen.de/~TMAP

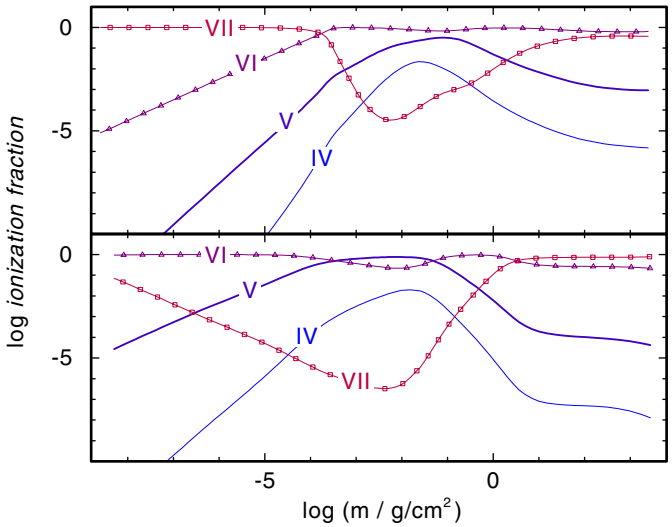

Fig. 1. Ga ionization fractions in our models for G191−B2B (*top panel*, H+Ga model) and RE 0503−289 (*bottom panel*, He+Ga).

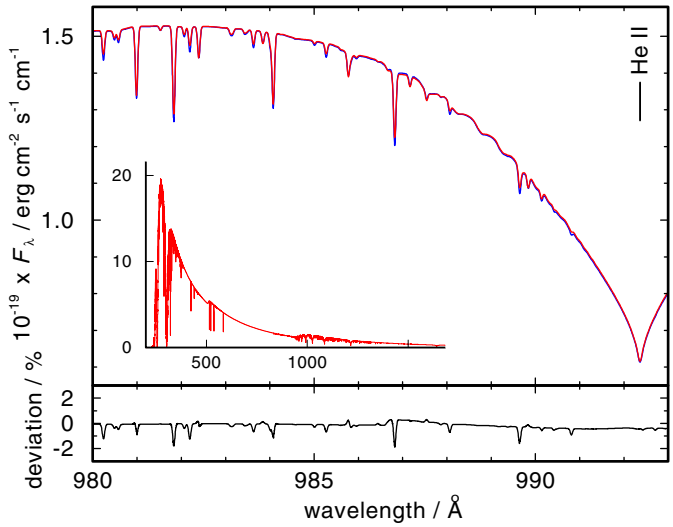

Fig. 2. *Top*: comparison of two SEDs from He+Ga composed model-atmospheres ($T_{\rm eff}$ = 70 000 K, $\log g$ = 7.5, 100 times solar Ga abundance), on the one hand calculated with a classical (thick, blue in the online version) and on the other hand with a statistical (thin, red) Ga model atom. The SEDs are convolved with a Gaussian ($FWHM$ = 0.06 Å) to simulate the FUSE resolution. *Inset*: wider wavelength range (statistical Ga model atom only). *Bottom*: $\left(F_\lambda^{\rm statistical}/F_\lambda^{\rm classical}\right) - 1$ illustrates the deviation between the two fluxes.

To represent the elements with an atomic number <20 with sufficient detail, we took the prepared ("classical") model atoms that are provided by the Tübingen Model-Atom Database (TMAD[4], Rauch & Deetjen 2003). TMAD was constructed in the framework of the German Astrophysical Virtual Observatory (GAVO[5]).

We decided to construct the model atoms for the trans-iron elements similar to those of Ca to Ni (Rauch & Deetjen 2003). To reduce the number of atomic levels and spectral lines considered in our model-atmosphere calculations, we employed our program Iron Opacity and Interface (IrOnIc, Rauch & Deetjen 2003), which uses a statistical approach to calculate so-called super levels and super lines. Table 10 demonstrates the strongly extenuated level and line numbers for Ga.

IrOnIc was designed to read data in the Kurucz format[6] (Kurucz 1991) as well as in the Opacity Project format[7]. We transferred our Zn, Ga, Ge, and Ba data into Kurucz-formatted files that were then ingested and processed by IrOnIc. The "statistical" model atoms that are created by this means were then used together with the "classical" model atoms for the lighter metals (see above) in our model atmosphere calculations.

To verify the reliability of this approach, we calculated models that consider only H+Ga and He+Ga with a 100 times solar Ga abundance (mass fraction 5.6×10^{-6}, solar value from Asplund et al. 2009) for G191−B2B ($T_{\rm eff}$ = 60 000 K, $\log g$ = 7.6) and RE 0503−289 ($T_{\rm eff}$ = 70 000 K, $\log g$ = 7.5). Figure 1 displays the Ga ionization fractions in these models. Ga V–VI are the dominant ionization stages in the line-forming region ($-4 \lesssim \log m \lesssim 0.5$). m is the column mass, measured from the outer boundary of our model atmospheres.

Figure 2 shows a good agreement between two SEDs from models computed with a classical and a statistical Ga model atom. The continuum flux level is matched exactly, while deviations (of about 1%) are visible at the line locations. The reason is simply the difference in the frequency grids (Rauch & Deetjen 2003). For classical model atoms, all spectral lines have a very narrow frequency discretization around their centers, while IrOnIc uses a line-independent frequency grid for its opacity-sampling method (Rauch & Deetjen 2003) that is equidistant in λ, for example.

For G191−B2B and RE 0503−289, TMAP uses a frequency grid within 50 Å $\le \lambda \le$ 300 000 Å with about 60 000 frequency points. Figure 2 (the inset) shows that the flux maximum in the model for RE 0503−289 is located around λ = 300 Å. In this region, we use a grid spacing of $\Delta\lambda = 5 \times 10^{-3}$ Å, while around λ = 1000 Å (about a factor of ten below the flux maximum), this is reduced to $\Delta\lambda = 1 \times 10^{-2}$ Å and, hence, the centers of the very narrow Ga lines do not match perfectly. To calculate synthetic spectra within a restricted wavelength range, for instance for FUSE (910 Å < λ < 1188 Å) and STIS (1150 Å < λ < 1780 Å), we use much finer frequency grids that, for example, consider the centers of Ga lines in detail (with 149 064 and 191 267 frequency points, respectively), and the SED agreement is even better.

For both stars, the final models of Rauch et al. (2014b) are adopted as start models for our calculations. For G191−B2B and RE 0503−289, the statistics of our model atoms are summarized in Tables 11 and 12, the model abundances in Tables 13 and 14.

The SEDs calculated for this analysis are available via the registered Theoretical Stellar Spectra Access (TheoSSA[8]) Virtual Observatory (VO) service.

5. Photospheric Ga abundances in G191−B2B and RE 0503−289

At a Ga abundance of 3.5×10^{-5} (mass fraction, 625 times the solar value), we were able to reproduce the identified Ga V lines (Table 15) in the FUSE spectrum of RE 0503−289 (Fig. 3).

[4] http://astro.uni-tuebingen.de/~TMAD

[5] http://www.g-vo.org

[6] GFxxyy.GAM, GFxxyy.LIN, and GFxxyy.POS files with xx = element number, yy = element charge, http://kurucz.harvard.edu/atoms.html

[7] http://cdsweb.u-strasbg.fr/topbase/topbase.html

[8] http://dc.g-vo.org/theossa

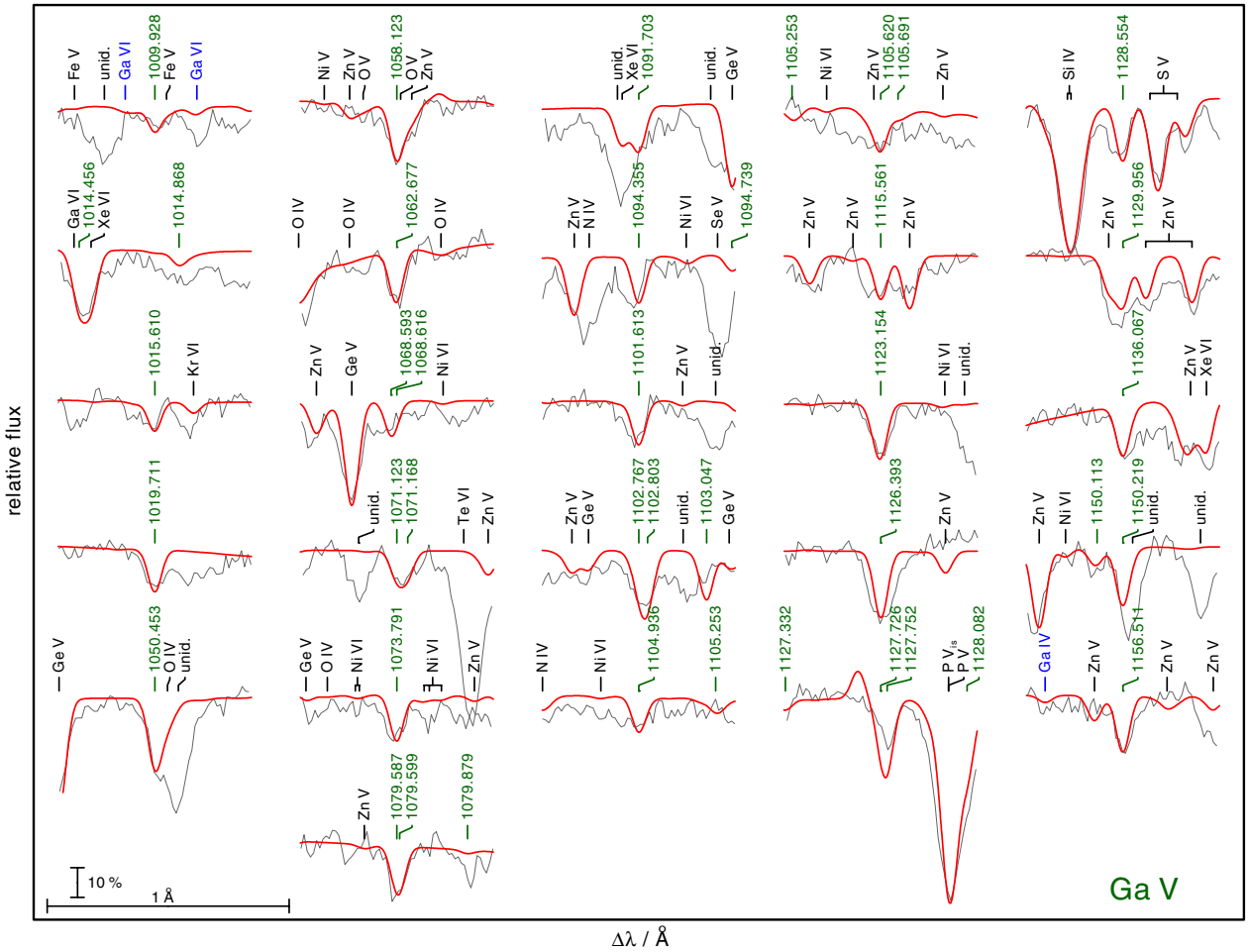

Fig. 3. Strongest Ga V lines in the FUSE observation of RE 0503−289, labeled (green in the online version) with their wavelengths from Table 8. The vertical bar indicates 10 % of the continuum flux. Identified lines are marked. "unid." denotes unidentified, "is" interstellar.

Table 10. Ga IV, Ga V, and Ga VI atomic levels and line transitions from Tables 7–9, respectively.

Ion	Atomic levels	Lines	Super levels	Super lines
IV	191	3198	7	19
V	91	517	7	15
VI	157	1914	7	13
	439	5629	21	47

Notes. The super levels and super lines are calculated by IrOnIc (Rauch & Deetjen 2003).

The search for Ga lines in the FUSE observation of G191−B2B was entirely negative. Our models for G191−B2B showed that the strongest Ga IV lines given by Shirai et al. (2007, with intensities of 1000) are located in the STIS wavelength range. These are Ga IV λ 1258.801 Å ($3d^9 4s\ ^3D_3$ – $3d^9 4p\ ^3F^o_4$), Ga IV λ 1303.540 Å ($3d^9 4s\ ^3D_2$ – $3d^9 4p\ ^3F^o_3$), and Ga IV λ 1338.129 Å ($3d^9 4s\ ^3D_3$ – $3d^9 4p\ ^3P^o_2$). They have the largest equivalent widths of all Ga lines in our models for G191−B2B and are positively identified in the STIS observation (Fig. 4). Ga IV λ 1303.540 Å is a blend with Fe V lines and, thus, uncertain, while the other two lines are isolated. We can reproduce their observed strengths at an abundance of 2.0×10^{-6} (by mass, 37 times solar, Fig. 4). At this abundance, four of the next strongest Ga IV lines (Ga IV $\lambda\lambda$ 1170.585, 1190.866, 1295.881, 1299.476 Å, with intensities of 220, 220, 650, and 600, respectively, Shirai et al. 2007) can also be identified and modeled, but they appear just above the noise level (Fig. 5). However, no detectable Ga line is predicted by our models in the FUSE wavelength range.

Ga IV $\lambda\lambda$ 1258.801, 1303.540, 1338.129 Å are also visible in the STIS observation of RE 0503−289 (Fig. 4) and agree well with the Ga abundance (3.5×10^{-5} by mass) determined from the FUSE spectrum.

6. Results and conclusions

We have unambiguously identified Ga V lines in the observed high-resolution UV spectra of G191−B2B and RE 0503−289. These lines are well reproduced by our NLTE model-atmosphere calculations using our newly calculated Ga IV–VI oscillator strengths.

We determined photospheric abundances of log Ga = −5.69 ± 0.2 (mass fraction, $1.7–2.5 \times 10^{-6}$, 30–44 times the solar abundance) and log Ga = −4.49 ± 0.1 ($3.0–4.0 \times 10^{-5}$, 536–715 times solar) for the DA-type white dwarf G191−B2B and the DO-type white dwarf RE 0503−289, respectively. These highly supersolar Ga abundances agree with the

Table 13. Photospheric abundances of G191−B2B as used in our final model.

Element	Mass Fraction	Number Fraction	[X]
H	9.99×10^{-1}	0.99998	0.132
He[a]	1.98×10^{-5}	5.0×10^{-6}	−4.099
C	6.31×10^{-6}	5.3×10^{-7}	−2.574
N	2.08×10^{-6}	1.5×10^{-7}	−2.522
O	1.90×10^{-5}	1.2×10^{-6}	−2.479
Al	1.12×10^{-5}	4.2×10^{-7}	−0.695
Si	5.29×10^{-5}	1.9×10^{-6}	−1.099
P	1.54×10^{-6}	5.0×10^{-8}	−0.579
S	5.72×10^{-6}	1.8×10^{-7}	−1.733
IG[b]	1.78×10^{-6}	4.0×10^{-8}	−1.558
Fe	6.50×10^{-4}	1.2×10^{-5}	−0.298
Ni	3.84×10^{-5}	6.6×10^{-7}	−0.269
Zn	3.50×10^{-6}	5.4×10^{-8}	0.304
Ga	2.00×10^{-6}	3.0×10^{-8}	1.560
Ge	3.24×10^{-6}	4.5×10^{-8}	1.135
Sn	3.53×10^{-7}	3.0×10^{-9}	2.588
Ba	4.00×10^{-6}	2.9×10^{-8}	3.495

Notes. [X] denotes log (abundance/solar abundance) of species X. [(a)] Upper limit given by Rauch et al. (2013). [(b)] Generic model atom (Rauch & Deetjen 2003) that comprises Ca, Sc, V, Ti, Cr, Mn, and Co, constructed with a relative abundance pattern that uses the upper abundance limits of Ti, Cr, Mn, and Co given by Rauch et al. (2013) and 1.0×10^{-7} (mass fraction) for Ca, Sc, and V.

Table 14. Same as Table 13, for RE 0503−289.

Element	Mass Fraction	Number Fraction	[X]
He	9.75×10^{-1}	9.9×10^{-1}	0.592
C	2.23×10^{-2}	7.6×10^{-3}	0.974
N	1.73×10^{-4}	5.0×10^{-5}	−0.602
O	1.97×10^{-3}	5.0×10^{-4}	−0.464
Si	1.61×10^{-4}	2.3×10^{-5}	−0.617
P	1.15×10^{-6}	1.5×10^{-7}	−0.705
S	3.97×10^{-5}	5.0×10^{-6}	−0.892
IG	1.00×10^{-6}	9.1×10^{-8}	−1.807
Fe	1.30×10^{-5}	9.5×10^{-7}	−1.997
Ni	7.26×10^{-5}	5.0×10^{-6}	0.008
Zn	1.13×10^{-4}	7.1×10^{-6}	1.814
Ga	3.45×10^{-5}	2.0×10^{-6}	2.790
Ge	1.59×10^{-4}	8.9×10^{-6}	2.825
Kr	5.05×10^{-5}	2.5×10^{-6}	2.666
Xe	6.30×10^{-5}	1.9×10^{-6}	4.732
Ba	3.58×10^{-4}	1.1×10^{-5}	5.447

high abundances of other trans-iron elements in G191−B2B and RE 0503−289 (Fig. 6).

The Ga IV/Ga V ionization balance is well reproduced in RE 0503−289 (Figs. 4, 5).

The identification of lines of Ga and its precise abundance determination became possible only because reliable transition probabilities for Ga IV, Ga V, and Ga VI were computed. Analogous calculations for other highly ionized trans-iron elements are very desirable. The precise measurement of their spectra, that is, their line wavelengths and relative strengths, as well as the determination of level energies and the calculation of transition probabilities remains a challenge for atomic and theoretical physicists.

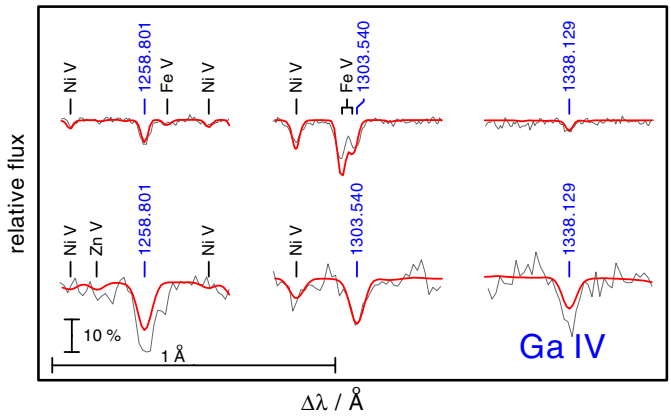

Fig. 4. Strongest Ga IV lines in the STIS observations of G191−B2B (*top*) and RE 0503−289 (*bottom*), labeled (blue in the online version) with their wavelengths from Table 7. Identified lines of other species are marked.

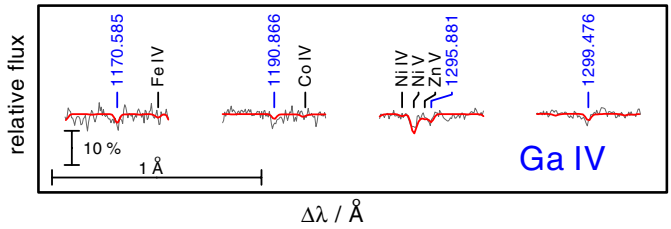

Fig. 5. Weaker Ga IV lines in the STIS observation of G191−B2B, labeled (blue in the online version) with their wavelengths from Table 7. Identified lines of other species are marked.

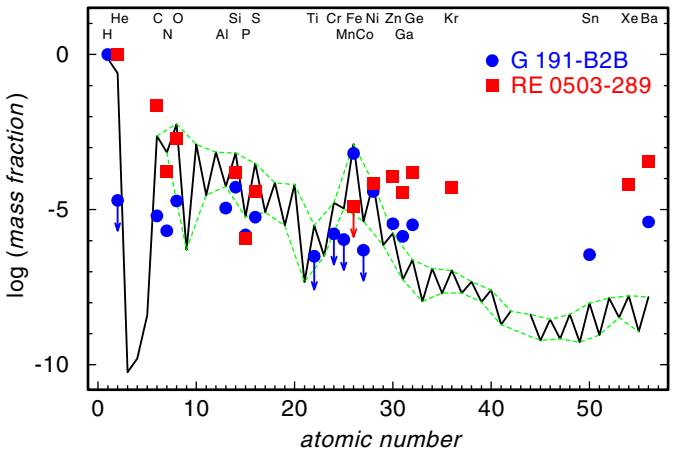

Fig. 6. Solar abundances (Asplund et al. 2009, thick line; the dashed lines connect the elements with even and with odd atomic number) compared with the determined photospheric abundances of G191−B2B (blue circles, Rauch et al. 2013) and RE 0503−289 (red squares, Dreizler & Werner 1996; Werner et al. 2012; Rauch et al. 2013, 2014a,b, and this work). The uncertainties of the WD abundances are about 0.2 dex in general. Arrows indicate upper limits.

Acknowledgements. T.R. is supported by the German Aerospace Center (DLR, grant 05 OR 1402). Financial support from the Belgian FRS-FNRS is also acknowledged. P.Q. is research director of this organization. This research has made use of the SIMBAD database, operated at CDS, Strasbourg, France. Some of the data presented in this paper were obtained from the Mikulski Archive for Space Telescopes (MAST). STScI is operated by the Association of Universities

for Research in Astronomy, Inc., under NASA contract NAS5-26555. Support for MAST for non-HST data is provided by the NASA Office of Space Science via grant NNX09AF08G and by other grants and contracts.

References

Aksenov, V. P., & Ryabtsev, A. N. 1974, Opt. Spectr., 37, 492
Asplund, M., Grevesse, N., Sauval, A. J., & Scott, P. 2009, ARA&A, 47, 481
Cowan, R. D. 1981, The theory of atomic structure and spectra (Berkeley, CA: University of California Press)
Dick, K. A. 1974, J. Opt. Soc. Am. (1917-1983), 64, 702
Dreizler, S., & Werner, K. 1996, A&A, 314, 217
Joshi, Y. N., Bhatia, K. S., & Jones, W. E. 1972, Sci. Light, 21, 113
Kononov, E. Y. 1967, Opt. Spectr., 23, 90
Kurucz, R. L. 1991, in Stellar Atmospheres – Beyond Classical Models, eds. L. Crivellari, I. Hubeny, & D. G. Hummer, NATO ASIC Proc., 341, 441
Mack, J. E., Laporte, O., & Lang, R. J. 1928, Phys. Rev., 31, 748
Moore, C. E. 1971, Atomic Energy Levels, Natl. Stand. Ref. Data Ser., Natl. Bur. Stand. (US), 35/Vol. II
Podobedova, L. I., Ryabtsev, A. N., & Ramonas, A. A. 1983, Sov. Phys. Collect., 23, 10
Podobedova, L. I., Ramonas, A. A., & Ryabtsev, A. N. 1985, Sov. Phys. Collect., 25, 66
Ramonas, A., & Ryabtsev, A. N. 1990, Lith. Phys. J., 37
Rauch, T., & Deetjen, J. L. 2003, in Stellar Atmosphere Modeling, eds. I. Hubeny, D. Mihalas, & K. Werner, ASP Conf. Ser., 288, 103
Rauch, T., Werner, K., Biémont, É., Quinet, P., & Kruk, J. W. 2012, A&A, 546, A55
Rauch, T., Werner, K., Bohlin, R., & Kruk, J. W. 2013, A&A, 560, A106
Rauch, T., Werner, K., Quinet, P., & Kruk, J. W. 2014a, A&A, 564, A41
Rauch, T., Werner, K., Quinet, P., & Kruk, J. W. 2014b, A&A, 566, A10
Ryabtsev, A. N. 1975, Opt. Spectr., 39, 455
Ryabtsev, A. N., & Churilov, S. S. 1991, Spectroscopy of Multicharged Ions in Hot Plasmas, ed. U. I. Safronova (Akad. Nauk. SSSR. Inst. Spektrosk. Moscow)
Ryabtsev, A. N., & Ramonas, A. 1985, Sov. Phys. Collect., 25, 77
Sawyer, R. A., & Humphreys, C. J. 1928, Phys. Rev., 32, 583
Shirai, T., Reader, J., Kramida, A. E., & Sugar, J. 2007, J. Phys. Chem. Ref. Data, 36, 509
van Deurzen, C. H. H. 1977, J. Opt. Soc. Am., 67, 476
Werner, K., Deetjen, J. L., Dreizler, S., et al. 2003, in Stellar Atmosphere Modeling, eds. I. Hubeny, D. Mihalas, & K. Werner, ASP Conf. Ser., 288, 31
Werner, K., Rauch, T., Ringat, E., & Kruk, J. W. 2012, ApJ, 753, L7

Pages 7 to 20 are available in the electronic edition of the journal at http://www.aanda.org

Table 1. Radial parameters (in cm^{-1}) adopted for the calculations in Ga IV.

Configuration	Parameter	HFR	Fitted	Ratio	Note
		Even parity			
$3d^{10}$	E_{av}	5814	5776		
$3d^9 4s$	E_{av}	148 422	156 111		
	ζ_{3d}	1407	1429	1.016	
	G^2(3d,4s)	12 329	11 238	0.912	
$3d^9 5s$	E_{av}	339 474	345 159		
	ζ_{3d}	1417	1428	1.008	
	G^2(3d,5s)	2908	2788	0.959	
$3d^9 6s$	E_{av}	408 900	414 843		
	ζ_{3d}	1419	1420	1.001	
	G^2(3d,6s)	1188	1373	1.155	
$3d^9 7s$	E_{av}	442 172	448 263		
	ζ_{3d}	1419	1433	1.010	
	G^2(3d,7s)	610	602	0.987	
$3d^9 4d$	E_{av}	328 479	337 724		
	ζ_{3d}	1416	1383	0.977	
	ζ_{4d}	80	80	1.000	F
	F^2(3d,4d)	12 570	10 395	0.827	
	F^4(3d,4d)	5095	5736	1.126	
	G^0(3d,4d)	4565	3720	0.815	R1
	G^2(3d,4d)	4572	3725	0.815	R1
	G^4(3d,4d)	3310	2697	0.815	R1
$3d^9 5d$	E_{av}	405 047	411 209		
	ζ_{3d}	1418	1428	1.007	
	ζ_{5d}	36	36	1.000	F
	F^2(3d,5d)	4880	5336	1.093	
	F^4(3d,5d)	2065	2372	1.149	
	G^0(3d,5d)	1843	1080	0.586	R2
	G^2(3d,5d)	1921	1125	0.586	R2
	G^4(3d,5d)	1411	826	0.586	R2
$3d^9 6d$	E_{av}	440 279	446 459		
	ζ_{3d}	1419	1471	1.037	
	ζ_{6d}	19	19	1.000	F
	F^2(3d,6d)	2451	2883	1.176	
	F^4(3d,6d)	1064	450	0.423	
	G^0(3d,6d)	939	332	0.353	R3
	G^2(3d,6d)	997	352	0.353	R3
	G^4(3d,6d)	736	260	0.353	R3
		Odd parity			
$3d^9 4p$	E_{av}	226 352	234 585		
	ζ_{3d}	1410	1436	1.019	
	ζ_{4p}	1471	1703	1.158	
	F^2(3d,4p)	24 145	23 088	0.956	
	G^1(3d,4p)	8521	7610	0.893	
	G^3(3d,4p)	7597	7510	0.989	
$3d^9 5p$	E_{av}	366 254	372 016		
	ζ_{3d}	1417	1431	1.010	
	ζ_{5p}	511	578	1.131	
	F^2(3d,5p)	7351	7159	0.974	
	G^1(3d,5p)	2389	2224	0.931	
	G^3(3d,5p)	2267	2375	1.047	
$3d^9 6p$	E_{av}	421 207	427 206		
	ζ_{3d}	1419	1430	1.008	
	ζ_{6p}	239	239	1.000	F
	F^2(3d,6p)	3232	3239	1.002	
	G^1(3d,6p)	1048	992	0.947	
	G^3(3d,6p)	1012	1055	1.043	
$3d^9 4f$	E_{av}	393 407	400 426		
	ζ_{3d}	1420	1433	1.009	
	ζ_{4f}	1	1	1.000	F
	F^2(3d,4f)	3960	3640	0.919	
	F^4(3d,4f)	932	775	0.832	
	G^1(3d,4f)	796	646	0.812	R4
	G^3(3d,4f)	452	367	0.812	R4
	G^5(3d,4f)	309	250	0.812	R4
$3d^8 4s4p$	E_{av}	423 926	438 259		
	F^2(3d,3d)	134 652	116 372	0.864	
	F^4(3d,3d)	84 593	73 554	0.870	
	α	0	93		
	ζ_{3d}	1508	1532	1.015	
	ζ_{4p}	1724	1941	1.126	
	F^2(3d,4p)	25 967	25 518	0.983	
	G^2(3d,4s)	12 383	10 647	0.860	
	G^1(3d,4p)	8854	8463	0.956	
	G^3(3d,4p)	8070	7998	0.991	
	G^1(4s,4p)	67 204	55 582	0.827	

Notes. F: parameter fixed to its ab initio value; R1, R2, R3, R4: ratios of these parameters were fixed in the fitting process.

Table 2. Same as Table 1 for Ga V.

Configuration	Parameter	HFR	Fitted	Ratio	Note[a]
		Even parity			
$3d^9$	E_{av}	5908	5922		
	ζ_{3d}	1420	1434	1.010	
$3d^8 4s$	E_{av}	226 836	232 051		
	F^2(3d,3d)	135 437	119 585	0.883	
	F^4(3d,3d)	85 127	72 403	0.851	
	α	0	114		
	ζ_{3d}	1518	1540	1.015	
	G^2(3d,4s)	13 184	12 284	0.932	
		Odd parity			
$3d^8 4p$	E_{av}	316 757	322 989		
	F^2(3d,3d)	135 720	119 775	0.883	
	F^4(3d,3d)	85 320	73 863	0.866	
	α	0	96		
	ζ_{3d}	1521	1521	1.000	
	ζ_{4p}	1986	2159	1.087	
	F^2(3d,4p)	28 462	27 751	0.975	
	G^1(3d,4p)	9794	8860	0.905	
	G^3(3d,4p)	9010	9342	1.037	
$3d^8 4f$	E_{av}	530 983	537 129		
	F^2(3d,3d)	136 572	118 715	0.869	
	F^4(3d,3d)	85 899	73 817	0.859	
	α	0	100		
	ζ_{3d}	1533	1475	0.962	
	ζ_{4f}	2	2	1.000	F
	F^2(3d,4f)	7050	6292	0.893	R1
	F^4(3d,4f)	2047	1827	0.893	R1
	G^1(3d,4f)	2094	1226	0.585	R2
	G^3(3d,4f)	1196	700	0.585	R2
	G^5(3d,4f)	818	479	0.585	R2

Notes. [(a)] F: parameter fixed to its ab initio value; R1, R2: ratios of these parameters were fixed in the fitting process.

Table 3. Same as Table 1 for Ga VI.

Configuration	Parameter	HFR	Fitted	Ratio
		Even parity		
$3d^8$	E_{av}	20 524	20 236	
	F^2(3d,3d)	136 668	121 986	0.893
	F^4(3d,3d)	85 965	74 905	0.871
	α	0	113	
	β	0	–418	
	ζ_{3d}	1534	1548	1.009
$3d^7 4s$	E_{av}	327 549	330 704	
	F^2(3d,3d)	142 387	126 538	0.889
	F^4(3d,3d)	89 820	80 221	0.893
	α	0	116	
	β	0	–487	
	ζ_{3d}	1636	1639	1.002
	G^2(3d,4s)	13 953	12 922	0.926
		Odd parity		
$3d^7 4p$	E_{av}	428 286	432 648	
	F^2(3d,3d)	142 618	127 015	0.891
	F^4(3d,3d)	89 979	79 692	0.886
	α	0	117	
	β	0	–390	
	ζ_{3d}	1638	1650	1.007
	ζ_{4p}	2526	2910	1.152
	F^2(3d,4p)	32 439	31 430	0.969
	G^1(3d,4p)	10 953	9842	0.899
	G^3(3d,4p)	10 310	10 455	1.014

Table 4. Comparison between experimental and calculated energy levels in Ga IV.

E_{exp} [a]	E_{calc} [b]	ΔE	J	Leading components (in %) in LS coupling[c]
				Even parity
0.0	0	0	0	99 $3d^{10}\ ^1S$
149 512.1	149 518	−6	3	99 $3d^9 4s\ ^3D$
150 967.0	150 959	8	2	85 $3d^9 4s\ ^3D$ + 14 $3d^9 4s\ ^1D$
153 085.9	153 087	−1	1	99 $3d^9 4s\ ^3D$
156 024.7	156 026	−1	2	85 $3d^9 4s\ ^1D$ + 14 $3d^9 4s\ ^3D$
328 763.7	328 928	−164	1	91 $3d^9 4d\ ^3S$ + 6 $3d^9 4d\ ^3P$
332 554.3	332 406	149	5	99 $3d^9 4d\ ^3G$
332 730.5	332 582	149	4	58 $3d^9 4d\ ^3G$ + 41 $3d^9 4d\ ^1G$
332 757.5	332 749	8	2	76 $3d^9 4d\ ^3P$ + 19 $3d^9 4d\ ^3D$
332 826.8	332 899	−72	1	46 $3d^9 4d\ ^1P$ + 31 $3d^9 4d\ ^3P$ + 22 $3d^9 4d\ ^3D$
333 964.2	333 770	194	3	90 $3d^9 4d\ ^3D$
334 403.3	334 393	10	0	98 $3d^9 4d\ ^3P$
334 527.6	334 931	−403	4	45 $3d^9 4d\ ^3F$ + 33 $3d^9 4d\ ^1G$ + 18 $3d^9 4d\ ^3G$
334 532.0	334 514	18	3	58 $3d^9 4d\ ^3G$ + 24 $3d^9 4d\ ^1F$ + 14 $3d^9 4d\ ^3F$
334 851.3	334 842	9	2	50 $3d^9 4d\ ^3D$ + 25 $3d^9 4d\ ^1D$ + 11 $3d^9 4d\ ^3P$
335 199.3	335 215	−16	1	54 $3d^9 4d\ ^3P$ + 37 $3d^9 4d\ ^1P$ + 8 $3d^9 4d\ ^3S$
336 581.6	336 527	54	3	41 $3d^9 4d\ ^3G$ + 39 $3d^9 4d\ ^1F$ + 17 $3d^9 4d\ ^3F$
336 790.0	336 893	−103	4	49 $3d^9 4d\ ^3F$ + 25 $3d^9 4d\ ^1G$ + 24 $3d^9 4d\ ^3G$
336 933.8	336 632	301	1	77 $3d^9 4d\ ^3D$ + 15 $3d^9 4d\ ^1P$ + 7 $3d^9 4d\ ^3P$
337 833.8	337 720	113	2	54 $3d^9 4d\ ^1D$ + 25 $3d^9 4d\ ^3D$ + 10 $3d^9 4d\ ^3P$
338 504.4	338 655	−150	3	56 $3d^9 4d\ ^3F$ + 32 $3d^9 4d\ ^1F$ + 8 $3d^9 4d\ ^3D$
338 719.6	338 835	−115	2	76 $3d^9 4d\ ^3F$ + 15 $3d^9 4d\ ^1D$ + 5 $3d^8 4s^2\ ^3F$
343 319.9	343 325	−5	3	99 $3d^9 5s\ ^3D$
343 912.7	343 908	5	2	55 $3d^9 5s\ ^3D$ + 44 $3d^9 5s\ ^1D$
346 887.6	346 885	3	1	99 $3d^9 5s\ ^3D$
347 402.8	347 407	−4	2	55 $3d^9 5s\ ^1D$ + 44 $3d^9 5s\ ^3D$
355 225.3	355 225	0	0	79 $3d^9 4d\ ^1S$ + 9 $3d^9 5d\ ^1S$ + 8 $3d^8 4s^2\ ^3P$
407 846.0	407 914	−68	1	79 $3d^9 5d\ ^3S$ + 15 $3d^9 5d\ ^3P$ + 6 $3d^9 5d\ ^1P$
409 158.0	409 134	24	5	100 $3d^9 5d\ ^3G$
409 280.0	409 177	103	4	50 $3d^9 5d\ ^1G$ + 50 $3d^9 5d\ ^3G$
409 303.0	409 342	−39	1	50 $3d^9 5d\ ^1P$ + 25 $3d^9 5d\ ^3D$ + 24 $3d^9 5d\ ^3P$
409 319.0	409 327	−8	2	72 $3d^9 5d\ ^3P$ + 26 $3d^9 5d\ ^3D$
409 716.0	409 775	−59	3	84 $3d^9 5d\ ^3D$ + 12 $3d^9 5d\ ^3F$
410 107.0	410 192	−85	3	48 $3d^9 5d\ ^1F$ + 31 $3d^9 5d\ ^3F$ + 21 $3d^9 5d\ ^3G$
410 220.0	410 268	−48	4	80 $3d^9 5d\ ^3F$ + 12 $3d^9 5d\ ^1G$ + 8 $3d^9 5d\ ^3G$
410 264.0	410 084	180	2	51 $3d^9 5d\ ^1D$ + 27 $3d^9 5d\ ^3D$ + 16 $3d^9 5d\ ^3F$
411 044.0	411 050	−6	0	97 $3d^9 5d\ ^3P$
412 243.0	412 255	−12	1	51 $3d^9 5d\ ^3P$ + 28 $3d^9 5d\ ^1P$ + 21 $3d^9 5d\ ^3S$
412 803.0	412 812	−9	3	79 $3d^9 5d\ ^3G$ + 13 $3d^9 5d\ ^1F$ + 8 $3d^9 5d\ ^3F$
413 010.0	413 054	−44	1	74 $3d^9 5d\ ^3D$ + 16 $3d^9 5d\ ^1P$ + 9 $3d^9 5d\ ^3P$
413 074.0	412 978	96	4	42 $3d^9 5d\ ^3G$ + 38 $3d^9 5d\ ^1G$ + 19 $3d^9 5d\ ^3F$
413 187.0	413 203	−16	3	96 $3d^9 6s\ ^3D$
413 198.0	413 174	24	2	30 $3d^9 5d\ ^3D$ + 23 $3d^9 5d\ ^1D$ + 17 $3d^9 5d\ ^3P$
413 661.0	413 645	16	2	39 $3d^9 6s\ ^1D$ + 33 $3d^9 6s\ ^3D$ + 14 $3d^9 5d\ ^3D$
413 832.0	413 905	−73	3	47 $3d^9 5d\ ^3F$ + 34 $3d^9 5d\ ^1F$ + 15 $3d^9 5d\ ^3D$
413 902.0	413 871	31	2	81 $3d^9 5d\ ^3F$ + 16 $3d^9 5d\ ^1D$
416 796.0	416 776	20	1	99 $3d^9 6s\ ^3D$
416 982.0	417 002	−20	2	52 $3d^9 6s\ ^3D$ + 47 $3d^9 6s\ ^1D$
419 737.0	419 746	−9	0	72 $3d^9 5d\ ^1S$ + 17 $3d^9 6d\ ^1S$
444 089.0	444 188	−99	1	66 $3d^9 6d\ ^3S$ + 25 $3d^9 6d\ ^3P$ + 8 $3d^9 6d\ ^1P$
444 706.0	444 674	32	5	100 $3d^9 6d\ ^3G$
444 765.0	444 688	77	1	53 $3d^9 6d\ ^1P$ + 25 $3d^9 6d\ ^3D$ + 22 $3d^9 6d\ ^3P$
444 767.0	444 663	104	4	53 $3d^9 6d\ ^1G$ + 46 $3d^9 6d\ ^3G$
444 783.0	444 674	109	2	74 $3d^9 6d\ ^3P$ + 21 $3d^9 6d\ ^3D$
444 979.0	445 069	−90	3	80 $3d^9 6d\ ^3D$ + 15 $3d^9 6d\ ^3F$
445 193.0	445 243	−50	3	53 $3d^9 6d\ ^1F$ + 31 $3d^9 6d\ ^3F$ + 14 $3d^9 6d\ ^3G$
445 234.0	445 156	78	2	52 $3d^9 6d\ ^1D$ + 28 $3d^9 6d\ ^3D$ + 18 $3d^9 6d\ ^3F$
445 236.0	445 269	−33	4	86 $3d^9 6d\ ^3F$ + 8 $3d^9 6d\ ^1G$ + 6 $3d^9 6d\ ^3G$
446 071.0	446 283	−212	0	90 $3d^9 6d\ ^3P$ + 6 $3d^9 6d\ ^1S$
446 732.0	446 731	1	3	99 $3d^9 7s\ ^3D$
446 852.0	446 853	−1	2	56 $3d^9 7s\ ^1D$ + 43 $3d^9 7s\ ^3D$

Notes. Energies are given in cm^{-1}. [a] From Shirai et al. (2007). [b] This work. [c] Only the first three components that are larger than 5% are given.

Table 4. continued.

E_{exp} [a]	E_{calc} [b]	ΔE	J	Leading components (in %) in LS coupling[c]
448 059.0	448 029	30	1	43 $3d^9 6d\ ^3P$ + 33 $3d^9 6d\ ^3S$ + 23 $3d^9 6d\ ^1P$
448 347.0	448 388	−41	3	86 $3d^9 6d\ ^3G$ + 9 $3d^9 6d\ ^1F$ + 5 $3d^9 6d\ ^3F$
448 482.0	448 540	−58	1	74 $3d^9 6d\ ^3D$ + 16 $3d^9 6d\ ^1P$ + 9 $3d^9 6d\ ^3P$
448 527.0	448 453	74	4	47 $3d^9 6d\ ^3G$ + 39 $3d^9 6d\ ^1G$ + 14 $3d^9 6d\ ^3F$
448 734.0	448 631	103	2	45 $3d^9 6d\ ^3D$ + 30 $3d^9 6d\ ^1D$ + 24 $3d^9 6d\ ^3P$
448 913.0	448 973	−60	3	47 $3d^9 6d\ ^3F$ + 35 $3d^9 6d\ ^1F$ + 17 $3d^9 6d\ ^3D$
448 964.0	448 946	18	2	81 $3d^9 6d\ ^3F$ + 13 $3d^9 6d\ ^1D$ + 6 $3d^9 6d\ ^3D$
450 316.0	450 315	1	1	99 $3d^9 7s\ ^3D$
450 405.0	450 406	−1	2	57 $3d^9 7s\ ^3D$ + 43 $3d^9 7s\ ^1D$
450 795.0	450 781	14	0	52 $3d^9 6d\ ^1S$ + 32 $3d^9 7d\ ^1S$ + 10 $3d^9 6d\ ^3P$
				Odd parity
224 243.3	224 311	−67	2	96 $3d^9 4p\ ^3P$
227 320.4	227 340	−20	1	96 $3d^9 4p\ ^3P$
227 681.2	227 655	27	3	68 $3d^9 4p\ ^3F$ + 27 $3d^9 4p\ ^1F$
228 952.8	228 891	62	4	99 $3d^9 4p\ ^3F$
229 140.3	229 131	10	0	99 $3d^9 4p\ ^3P$
230 040.0	230 003	37	2	94 $3d^9 4p\ ^3F$
233 192.3	233 213	−21	3	62 $3d^9 4p\ ^1F$ + 23 $3d^9 4p\ ^3D$ + 15 $3d^9 4p\ ^3F$
233 824.7	233 857	−33	2	62 $3d^9 4p\ ^1D$ + 33 $3d^9 4p\ ^3D$
234 939.5	234 889	50	3	73 $3d^9 4p\ ^3D$ + 16 $3d^9 4p\ ^3F$ + 10 $3d^9 4p\ ^1F$
236 311.9	236 303	9	1	66 $3d^9 4p\ ^1P$ + 33 $3d^9 4p\ ^3D$
236 906.5	236 923	−17	1	64 $3d^9 4p\ ^3D$ + 32 $3d^9 4p\ ^1P$
237 458.0	237 494	−36	2	59 $3d^9 4p\ ^3D$ + 37 $3d^9 4p\ ^1D$
368 684.0	368 705	−21	2	94 $3d^9 5p\ ^3P$ + 6 $3d^9 5p\ ^3D$
369 718.0	369 714	4	3	57 $3d^9 5p\ ^3F$ + 38 $3d^9 5p\ ^1F$ + 5 $3d^9 5p\ ^3D$
370 123.0	370 092	31	4	100 $3d^9 5p\ ^3F$
370 458.0	370 465	−7	1	72 $3d^9 5p\ ^3P$ + 22 $3d^9 5p\ ^1P$ + 6 $3d^9 5p\ ^3D$
371 295.0	371 306	−11	2	43 $3d^9 5p\ ^1D$ + 30 $3d^9 5p\ ^3D$ + 24 $3d^9 5p\ ^3F$
371 636.0	371 636	0	3	81 $3d^9 5p\ ^3D$ + 18 $3d^9 5p\ ^1F$
372 649.0	372 647	2	0	100 $3d^9 5p\ ^3P$
373 171.0	373 160	11	2	74 $3d^9 5p\ ^3F$ + 23 $3d^9 5p\ ^1D$
373 824.0	373 822	2	1	76 $3d^9 5p\ ^1P$ + 24 $3d^9 5p\ ^3P$
374 167.0	374 171	−4	3	44 $3d^9 5p\ ^1F$ + 42 $3d^9 5p\ ^3F$ + 14 $3d^9 5p\ ^3D$
374 883.0	374 870	13	1	94 $3d^9 5p\ ^3D$
375 134.0	375 154	−20	2	60 $3d^9 5p\ ^3D$ + 34 $3d^9 5p\ ^1D$
397 883.9	397 877	7	0	100 $3d^9 4f\ ^3P$
398 043.0	398 036	7	1	86 $3d^9 4f\ ^3P$ + 11 $3d^9 4f\ ^3D$
398 319.7	398 317	3	2	51 $3d^9 4f\ ^3P$ + 30 $3d^9 4f\ ^3D$ + 18 $3d^9 4f\ ^1D$
398 486.2	398 502	−15	6	100 $3d^9 4f\ ^3H$
398 489.8	398 513	−23	5	54 $3d^9 4f\ ^1H$ + 46 $3d^9 4f\ ^3H$
398 851.5	398 848	3	2	40 $3d^9 4f\ ^1D$ + 34 $3d^9 4f\ ^3F$ + 25 $3d^9 4f\ ^3D$
398 866.0	398 850	16	3	66 $3d^9 4f\ ^3D$ + 24 $3d^9 4f\ ^3F$ + 10 $3d^9 4f\ ^1F$
398 927.7	398 925	3	1	52 $3d^9 4f\ ^3D$ + 46 $3d^9 4f\ ^1P$
399 165.8	399 158	7	4	65 $3d^9 4f\ ^3F$ + 32 $3d^9 4f\ ^3G$
399 175.9	399 178	−2	5	82 $3d^9 4f\ ^3G$ + 9 $3d^9 4f\ ^3H$ + 9 $3d^9 4f\ ^1H$
399 181.0	399 186	−5	4	55 $3d^9 4f\ ^1G$ + 18 $3d^9 4f\ ^3G$ + 16 $3d^9 4f\ ^3H$
399 205.0	399 207	−2	3	47 $3d^9 4f\ ^1F$ + 29 $3d^9 4f\ ^3F$ + 24 $3d^9 4f\ ^3G$
401 836.6	401 828	9	2	49 $3d^9 4f\ ^3P$ + 31 $3d^9 4f\ ^3D$ + 20 $3d^9 4f\ ^1D$
402 191.0	402 208	−17	5	44 $3d^9 4f\ ^3H$ + 38 $3d^9 4f\ ^1H$ + 18 $3d^9 4f\ ^3G$
402 196.0	402 197	−1	4	82 $3d^9 4f\ ^3H$ + 10 $3d^9 4f\ ^1G$ + 8 $3d^9 4f\ ^3G$
402 353.4	402 355	−2	1	50 $3d^9 4f\ ^1P$ + 37 $3d^9 4f\ ^3D$ + 13 $3d^9 4f\ ^3P$
402 546.1	402 537	9	2	65 $3d^9 4f\ ^3F$ + 21 $3d^9 4f\ ^1D$ + 13 $3d^9 4f\ ^3D$
402 567.4	402 564	4	3	40 $3d^9 4f\ ^3F$ + 33 $3d^9 4f\ ^3D$ + 26 $3d^9 4f\ ^1F$
402 838.6	402 844	−5	4	42 $3d^9 4f\ ^3G$ + 35 $3d^9 4f\ ^1G$ + 23 $3d^9 4f\ ^3F$
402 844.6	402 841	3	3	75 $3d^9 4f\ ^3G$ + 17 $3d^9 4f\ ^1F$ + 8 $3d^9 4f\ ^3F$
403 072.0	403 051	21	4	90 $3d^8(^3F)4s4p\ ^5D$ + 5 $3d^8(^3P)4s4p\ ^5D$
405 366.0	405 403	−37	3	87 $3d^8(^3F)4s4p\ ^5D$ + 6 $3d^8(^3P)4s4p\ ^5D$
407 383.0	407 365	18	2	87 $3d^8(^3F)4s4p\ ^5D$ + 7 $3d^8(^3P)4s4p\ ^5D$
408 135.0	408 137	−2	4	78 $3d^8(^3F)4s4p\ ^5G$ + 11 $3d^8(^3F)4s4p\ ^5F$
412 166.0	412 133	33	4	79 $3d^8(^3F)4s4p\ ^5F$ + 10 $3d^8(^3F)4s4p\ ^5G$
413 211.0	413 183	28	3	81 $3d^8(^3F)4s4p\ ^5F$ + 8 $3d^8(^3F)4s4p\ ^5G$
413 850.0	413 845	5	2	87 $3d^8(^3F)4s4p\ ^5F$
414 099.0	414 131	−32	1	92 $3d^8(^3F)4s4p\ ^5F$

Table 4. continued.

E_{exp} [a]	E_{calc} [b]	ΔE	J	Leading components (in %) in LS coupling[c]
414 379.0	414 428	−49	4	40 $3d^8(^3F)4s4p\ ^3G$ + 25 $3d^8(^3F)4s4p\ ^1G$ + 21 $3d^8(^3F)4s4p\ ^3G$
415 296.0	415 349	−53	3	52 $3d^8(^3F)4s4p\ ^3D$ + 18 $3d^8(^3F)4s4p\ ^3D$ + 10 $3d^8(^3F)4s4p\ ^3F$
416 606.0	416 638	−32	3	56 $3d^8(^3F)4s4p\ ^3G$ + 29 $3d^8(^3F)4s4p\ ^3G$ + 6 $3d^8(^3F)4s4p\ ^3D$
416 647.0	416 676	−29	2	51 $3d^8(^3F)4s4p\ ^3D$ + 21 $3d^8(^3F)4s4p\ ^3D$ + 8 $3d^8(^3F)4s4p\ ^3F$
418 395.0	418 394	1	1	56 $3d^8(^3F)4s4p\ ^3D$ + 25 $3d^8(^3F)4s4p\ ^3D$ + 9 $3d^8(^1D)4s4p\ ^3D$
418 405.0	418 507	−102	4	54 $3d^8(^3F)4s4p\ ^3F$ + 34 $3d^8(^3F)4s4p\ ^3F$ + 5 $3d^8(^3F)4s4p\ ^5F$
419 057.0	419 107	−50	3	36 $3d^8(^3F)4s4p\ ^3F$ + 22 $3d^8(^3F)4s4p\ ^3F$ + 19 $3d^8(^3F)4s4p\ ^1F$
420 572.0	420 614	−42	2	51 $3d^8(^3F)4s4p\ ^3F$ + 29 $3d^8(^3F)4s4p\ ^3F$ + 8 $3d^8(^3F)4s4p\ ^3D$
420 623.0	420 636	−13	4	69 $3d^8(^3F)4s4p\ ^1G$ + 15 $3d^8(^3F)4s4p\ ^3G$ + 11 $3d^8(^3F)4s4p\ ^3G$
423 151.0	423 149	2	2	82 $3d^8(^3F)4s4p\ ^1D$
423 434.0	423 496	−62	3	70 $3d^8(^3F)4s4p\ ^1F$ + 9 $3d^8(^3F)4s4p\ ^3F$ + 7 $3d^8(^3F)4s4p\ ^3F$
424 901.0	424 934	−33	2	91 $3d^96p\ ^3P$ + 8 $3d^96p\ ^3D$
425 253.0	425 229	24	2	82 $3d^8(^3P)4s4p\ ^5P$ + 5 $3d^8(^3F)4s4p\ ^1D$
425 368.0	425 393	−25	3	51 $3d^96p\ ^3F$ + 42 $3d^96p\ ^1F$ + 5 $3d^96p\ ^3D$
425 552.0	425 522	30	4	100 $3d^96p\ ^3F$
425 604.0	425 561	43	3	83 $3d^8(^3P)4s4p\ ^5P$ + 6 $3d^8(^1D)4s4p\ ^3D$
425 702.0	425 624	78	1	93 $3d^8(^3P)4s4p\ ^5P$
425 853.0	425 849	4	1	48 $3d^96p\ ^3P$ + 43 $3d^96p\ ^1P$ + 8 $3d^96p\ ^3D$
426 175.0	426 178	−3	3	85 $3d^96p\ ^3D$ + 14 $3d^96p\ ^1F$
426 180.0	426 163	17	2	52 $3d^96p\ ^1D$ + 33 $3d^96p\ ^3D$ + 11 $3d^96p\ ^3F$
428 648.0	428 635	13	0	100 $3d^96p\ ^3P$
428 828.0	428 831	−3	2	84 $3d^96p\ ^3F$ + 11 $3d^96p\ ^1D$
429 003.0	429 015	−12	1	51 $3d^96p\ ^1P$ + 49 $3d^96p\ ^3P$
429 305.0	429 281	24	3	47 $3d^96p\ ^3F$ + 43 $3d^96p\ ^1F$ + 9 $3d^96p\ ^3D$
429 594.0	429 591	3	1	90 $3d^96p\ ^3D$ + 6 $3d^96p\ ^1P$
429 685.0	429 707	−22	2	52 $3d^96p\ ^3D$ + 34 $3d^96p\ ^1D$ + 5 $3d^96p\ ^3P$
429 866.0	429 879	−13	2	69 $3d^8(^1D)4s4p\ ^3F$ + 6 $3d^8(^1D)4s4p\ ^3D$ + 5 $3d^96p\ ^3D$
430 492.0	430 454	38	3	69 $3d^8(^1D)4s4p\ ^3F$ + 7 $3d^8(^3P)4s4p\ ^5D$ + 5 $3d^8(^1G)4s4p\ ^3F$
430 682.0	430 791	−109	1	49 $3d^8(^1D)4s4p\ ^3D$ + 15 $3d^8(^1D)4s4p\ ^3P$ + 11 $3d^8(^3F)4s4p\ ^3D$
431 242.0	431 358	−116	2	58 $3d^8(^1D)4s4p\ ^3D$ + 8 $3d^8(^1D)4s4p\ ^3F$ + 7 $3d^8(^3F)4s4p\ ^3D$
431 353.0	431 214	139	4	64 $3d^8(^1D)4s4p\ ^3F$ + 22 $3d^8(^3P)4s4p\ ^5D$ + 9 $3d^8(^1G)4s4p\ ^3F$
431 957.0	432 142	−185	3	72 $3d^8(^1D)4s4p\ ^3D$ + 7 $3d^8(^3P)4s4p\ ^5P$ + 5 $3d^8(^1D)4s4p\ ^3F$
432 846.0	432 714	132	1	43 $3d^8(^1D)4s4p\ ^3P$ + 30 $3d^8(^1D)4s4p\ ^3D$ + 11 $3d^8(^3P)4s4p\ ^3P$
433 778.0	433 683	95	2	67 $3d^8(^1D)4s4p\ ^3P$ + 14 $3d^8(^1D)4s4p\ ^3D$ + 5 $3d^8(^3P)4s4p\ ^3P$
434 722.0	434 587	135	2	84 $3d^8(^3P)4s4p\ ^5D$ + 7 $3d^8(^3F)4s4p\ ^5D$
434 846.0	434 911	−65	3	79 $3d^8(^3P)4s4p\ ^5D$ + 8 $3d^8(^1D)4s4p\ ^3F$ + 5 $3d^8(^3F)4s4p\ ^5D$
435 419.0	435 414	5	4	69 $3d^8(^3P)4s4p\ ^5D$ + 14 $3d^8(^1D)4s4p\ ^3F$ + 12 $3d^8(^1G)4s4p\ ^3F$
437 787.0	437 649	138	2	30 $3d^8(^3P)4s4p\ ^3P$ + 17 $3d^95f\ ^3P$ + 15 $3d^95f\ ^3D$
439 390.0	439 207	183	1	31 $3d^8(^3P)4s4p\ ^3P$ + 19 $3d^8(^1D)4s4p\ ^3P$ + 12 $3d^8(^3P)4s4p\ ^3D$
440 111.0	440 153	−42	2	34 $3d^8(^3P)4s4p\ ^3D$ + 18 $3d^8(^3P)4s4p\ ^3D$ + 11 $3d^8(^3P)4s4p\ ^3P$
440 188.0	440 281	−93	3	40 $3d^8(^3P)4s4p\ ^3D$ + 23 $3d^8(^3P)4s4p\ ^3D$ + 12 $3d^8(^3F)4s4p\ ^3D$
440 229.0	440 237	−8	1	39 $3d^8(^3P)4s4p\ ^3D$ + 19 $3d^8(^3P)4s4p\ ^3D$ + 11 $3d^8(^3P)4s4p\ ^1P$
440 723.0	440 581	142	0	46 $3d^8(^3P)4s4p\ ^3P$ + 37 $3d^8(^1D)4s4p\ ^3P$ + 11 $3d^8(^3P)4s4p\ ^3P$
441 367.0	441 414	−47	4	51 $3d^8(^1G)4s4p\ ^3F$ + 14 $3d^8(^1D)4s4p\ ^3F$ + 13 $3d^8(^3F)4s4p\ ^3F$
442 220.0	442 672	−452	3	47 $3d^8(^1G)4s4p\ ^3F$ + 10 $3d^8(^1D)4s4p\ ^3F$ + 9 $3d^95f\ ^3F$
442 837.0	442 870	−33	2	95 $3d^8(^3P)4s4p\ ^5S$
443 344.0	443 090	254	1	74 $3d^8(^3P)4s4p\ ^1P$ + 6 $3d^8(^3P)4s4p\ ^3P$ + 5 $3d^8(^1D)4s4p\ ^3P$
443 322.0	443 193	129	2	67 $3d^8(^1G)4s4p\ ^3F$ + 7 $3d^8(^1D)4s4p\ ^3F$ + 7 $3d^8(^3F)4s4p\ ^3F$
444 074.0	444 163	−89	3	54 $3d^8(^3F)4s4p\ ^3D$ + 20 $3d^8(^3F)4s4p\ ^3D$ + 9 $3d^8(^3P)4s4p\ ^3D$
444 348.0	444 392	−44	2	79 $3d^8(^3P)4s4p\ ^1D$
444 968.0	444 768	200	4	39 $3d^8(^3F)4s4p\ ^3G$ + 24 $3d^8(^3F)4s4p\ ^3G$ + 12 $3d^8(^3F)4s4p\ ^3F$
446 456.0	446 332	124	4	38 $3d^8(^3F)4s4p\ ^3F$ + 19 $3d^8(^3F)4s4p\ ^3F$ + 14 $3d^8(^3F)4s4p\ ^3G$
446 917.0	446 948	−31	2	55 $3d^8(^3F)4s4p\ ^3D$ + 22 $3d^8(^3F)4s4p\ ^3D$ + 8 $3d^8(^3P)4s4p\ ^3D$
447 014.0	446 771	243	3	52 $3d^8(^3F)4s4p\ ^3G$ + 29 $3d^8(^3F)4s4p\ ^3G$ + 5 $3d^8(^3F)4s4p\ ^3F$
448 614.0	448 611	3	1	58 $3d^8(^3F)4s4p\ ^3D$ + 25 $3d^8(^3F)4s4p\ ^3D$ + 7 $3d^8(^3P)4s4p\ ^3D$
448 773.0	448 704	69	3	49 $3d^8(^3F)4s4p\ ^3F$ + 25 $3d^8(^3F)4s4p\ ^3F$ + 8 $3d^8(^1G)4s4p\ ^3F$
450 162.0	450 142	20	2	55 $3d^8(^3F)4s4p\ ^3F$ + 27 $3d^8(^3F)4s4p\ ^3F$ + 7 $3d^8(^1G)4s4p\ ^3F$
462 491.0	462 616	−125	2	48 $3d^8(^1D)4s4p\ ^1D$ + 25 $3d^8(^3P)4s4p\ ^3P$ + 10 $3d^8(^3P)4s4p\ ^3P$
463 246.0	463 067	179	3	64 $3d^8(^1D)4s4p\ ^1F$ + 12 $3d^96f\ ^3G$ + 6 $3d^96f\ ^3D$
464 221.0	464 310	−89	1	43 $3d^8(^3P)4s4p\ ^3P$ + 28 $3d^8(^1D)4s4p\ ^1P$ + 15 $3d^8(^3P)4s4p\ ^3P$
465 833.0	466 138	−305	0	70 $3d^8(^3P)4s4p\ ^3P$ + 24 $3d^8(^3P)4s4p\ ^3P$
466 359.0	466 457	−98	2	38 $3d^8(^3P)4s4p\ ^3P$ + 37 $3d^8(^1D)4s4p\ ^1D$ + 16 $3d^8(^3P)4s4p\ ^3P$
467 778.0	467 884	−106	1	55 $3d^8(^1D)4s4p\ ^1P$ + 25 $3d^8(^3P)4s4p\ ^3P$ + 9 $3d^8(^3P)4s4p\ ^3P$
475 514.0	475 390	124	3	89 $3d^8(^1G)4s4p\ ^1F$

Table 5. Same as Table 6 for Ga V.

E_{exp} [a]	E_{calc} [b]	ΔE	J	Leading components (in %) in LS coupling[c]
				Even parity
0	0	0	2.5	99 $3d^9\ ^2D$
3583	3583	0	1.5	99 $3d^9\ ^2D$
210 052	210 053	−1	4.5	99 $3d^8(^3F)4s\ ^4F$
212 121	212 098	23	3.5	95 $3d^8(^3F)4s\ ^4F$
214 000	213 960	40	2.5	97 $3d^8(^3F)4s\ ^4F$
215 237	215 192	45	1.5	98 $3d^8(^3F)4s\ ^4F$
218 301	218 359	−58	3.5	94 $3d^8(^3F)4s\ ^2F$ + 5 $3d^8(^3F)4s\ ^4F$
221 488	221 535	−47	2.5	95 $3d^8(^3F)4s\ ^2F$
231 711	231 747	−36	2.5	50 $3d^8(^3P)4s\ ^4P$ + 47 $3d^8(^1D)4s\ ^2D$
232 968	232 897	71	1.5	76 $3d^8(^1D)4s\ ^2D$ + 16 $3d^8(^3P)4s\ ^4P$ + 5 $3d^8(^3P)4s\ ^2P$
235 609	235 639	−30	1.5	83 $3d^8(^3P)4s\ ^4P$ + 16 $3d^8(^1D)4s\ ^2D$
235 752	235 788	−36	0.5	99 $3d^8(^3P)4s\ ^4P$
236 072	236 137	−65	2.5	49 $3d^8(^1D)4s\ ^2D$ + 49 $3d^8(^3P)4s\ ^4P$
242 026	242 031	−5	1.5	94 $3d^8(^3P)4s\ ^2P$ + 5 $3d^8(^1D)4s\ ^2D$
243 053	242 952	101	0.5	99 $3d^8(^3P)4s\ ^2P$
246 093	246 107	−14	4.5	99 $3d^8(^1G)4s\ ^2G$
246 133	246 119	14	3.5	99 $3d^8(^1G)4s\ ^2G$
				Odd parity
296 992	297 189	−197	3.5	89 $3d^8(^3F)4p\ ^4D$
300 144	300 226	−82	2.5	87 $3d^8(^3F)4p\ ^4D$ + 6 $3d^8(^3P)4p\ ^4D$ + 5 $3d^8(^3F)4p\ ^4F$
300 730	300 780	−50	4.5	59 $3d^8(^3F)4p\ ^4G$ + 24 $3d^8(^3F)4p\ ^2G$ + 16 $3d^8(^3F)4p\ ^4F$
302 217	302 017	200	5.5	99 $3d^8(^3F)4p\ ^4G$
302 499	302 501	−2	1.5	89 $3d^8(^3F)4p\ ^4D$ + 7 $3d^8(^3P)4p\ ^4D$
302 779	302 709	70	3.5	77 $3d^8(^3F)4p\ ^4G$ + 12 $3d^8(^3F)4p\ ^4F$ + 9 $3d^8(^3F)4p\ ^2G$
303 911	303 863	48	0.5	90 $3d^8(^3F)4p\ ^4D$ + 8 $3d^8(^3P)4p\ ^4D$
304 272	304 148	124	2.5	90 $3d^8(^3F)4p\ ^4G$ + 6 $3d^8(^3F)4p\ ^4F$
305 249	305 168	81	4.5	80 $3d^8(^3F)4p\ ^4F$ + 13 $3d^8(^3F)4p\ ^2G$ + 6 $3d^8(^3F)4p\ ^4G$
306 628	306 546	82	3.5	64 $3d^8(^3F)4p\ ^4F$ + 20 $3d^8(^3F)4p\ ^2F$ + 10 $3d^8(^3F)4p\ ^4G$
306 947	306 903	44	4.5	62 $3d^8(^3F)4p\ ^2G$ + 35 $3d^8(^3F)4p\ ^4G$
307 745	307 661	84	2.5	73 $3d^8(^3F)4p\ ^4F$ + 11 $3d^8(^3F)4p\ ^2D$ + 7 $3d^8(^3F)4p\ ^4G$
307 864	307 869	−5	1.5	74 $3d^8(^3F)4p\ ^4F$ + 15 $3d^8(^3F)4p\ ^2D$ + 7 $3d^8(^1D)4p\ ^2D$
309 616	309 786	−170	2.5	68 $3d^8(^3F)4p\ ^2D$ + 14 $3d^8(^3F)4p\ ^2F$ + 7 $3d^8(^3F)4p\ ^4F$
309 679	309 741	−62	3.5	56 $3d^8(^3F)4p\ ^2G$ + 32 $3d^8(^3F)4p\ ^2F$ + 8 $3d^8(^3F)4p\ ^4F$
310 267	310 302	−35	3.5	44 $3d^8(^3F)4p\ ^2F$ + 33 $3d^8(^3F)4p\ ^2G$ + 11 $3d^8(^3F)4p\ ^4F$
311 991	312 107	−116	1.5	64 $3d^8(^3F)4p\ ^2D$ + 21 $3d^8(^3F)4p\ ^4F$ + 9 $3d^8(^1D)4p\ ^2D$
313 088	313 131	−43	2.5	76 $3d^8(^3F)4p\ ^2F$ + 12 $3d^8(^3F)4p\ ^2D$ + 8 $3d^8(^3F)4p\ ^4F$
319 570	319 643	−73	1.5	76 $3d^8(^3P)4p\ ^4P$ + 9 $3d^8(^1D)4p\ ^2P$
320 093	320 174	−81	2.5	72 $3d^8(^3P)4p\ ^4P$ + 12 $3d^8(^1D)4p\ ^2D$ + 7 $3d^8(^1D)4p\ ^2F$
320 429	320 437	−8	0.5	91 $3d^8(^3P)4p\ ^4P$
322 388	322 363	25	2.5	74 $3d^8(^1D)4p\ ^2F$ + 14 $3d^8(^3P)4p\ ^4P$
324 314	324 449	−135	1.5	44 $3d^8(^1D)4p\ ^2D$ + 17 $3d^8(^3P)4p\ ^4P$ + 15 $3d^8(^1D)4p\ ^2P$
324 407	324 224	183	3.5	75 $3d^8(^1D)4p\ ^2F$ + 11 $3d^8(^1G)4p\ ^2F$ + 10 $3d^8(^3P)4p\ ^4D$
324 874	324 765	109	0.5	61 $3d^8(^1D)4p\ ^2P$ + 28 $3d^8(^3P)4p\ ^2P$ + 7 $3d^8(^3P)4p\ ^4P$
325 713	325 904	−191	2.5	76 $3d^8(^1D)4p\ ^2D$ + 10 $3d^8(^3P)4p\ ^4P$
326 549	326 553	−4	1.5	50 $3d^8(^1D)4p\ ^2P$ + 32 $3d^8(^1D)4p\ ^2D$ + 7 $3d^8(^3P)4p\ ^2P$
329 103	329 093	10	2.5	66 $3d^8(^3P)4p\ ^4D$ + 18 $3d^8(^3P)4p\ ^2D$ + 5 $3d^8(^1D)4p\ ^2F$
329 108	329 021	87	0.5	88 $3d^8(^3P)4p\ ^4D$ + 8 $3d^8(^3F)4p\ ^4D$
329 112	329 020	92	1.5	79 $3d^8(^3P)4p\ ^4D$ + 6 $3d^8(^3F)4p\ ^4D$ + 6 $3d^8(^3P)4p\ ^2D$
330 174	330 058	116	3.5	80 $3d^8(^3P)4p\ ^4D$ + 10 $3d^8(^1G)4p\ ^2F$ + 5 $3d^8(^1D)4p\ ^2F$
332 473	332 531	−58	2.5	71 $3d^8(^3P)4p\ ^2D$ + 22 $3d^8(^3P)4p\ ^4D$
332 600	332 470	130	4.5	98 $3d^8(^1G)4p\ ^2H$
332 707	332 576	131	1.5	72 $3d^8(^3P)4p\ ^2P$ + 14 $3d^8(^1D)4p\ ^2P$ + 10 $3d^8(^3P)4p\ ^2D$
333 929	333 923	6	1.5	81 $3d^8(^3P)4p\ ^2D$ + 8 $3d^8(^3P)4p\ ^4D$ + 5 $3d^8(^3P)4p\ ^2P$
334 765	335 015	−250	5.5	99 $3d^8(^1G)4p\ ^2H$
335 089	335 167	−78	3.5	74 $3d^8(^1G)4p\ ^2F$ + 17 $3d^8(^1D)4p\ ^2F$
335 605	335 408	197	0.5	63 $3d^8(^3P)4p\ ^2P$ + 24 $3d^8(^1D)4p\ ^2P$ + 9 $3d^8(^3P)4p\ ^2S$
336 909	336 815	94	2.5	86 $3d^8(^1G)4p\ ^2F$ + 8 $3d^8(^1D)4p\ ^2F$
337 491	337 786	−295	0.5	89 $3d^8(^3P)4p\ ^2S$ + 6 $3d^8(^1D)4p\ ^2P$
337 690	337 741	−51	1.5	97 $3d^8(^3P)4p\ ^4S$
344 200	344 163	37	3.5	97 $3d^8(^1G)4p\ ^2G$

Notes. [a] From Shirai et al. (2007). [b] This work. [c] Only the first three components that are larger than 5% are given.

Table 5. continued.

E_{exp} [a]	E_{calc} [b]	ΔE	J	Leading components (in %) in LS coupling[c]
344 668	344 633	35	4.5	98 $3d^8(^1G)4p\ ^2G$
519 872	519 651	221	1.5	28 $3d^8(^3F)4f\ ^4P$ + 27 $3d^8(^3P)5p\ ^4P$ + 19 $3d^8(^3F)4f\ ^4S$
520 289	520 519	−230	3.5	45 $3d^8(^3F)4f\ ^2F$ + 18 $3d^8(^3F)4f\ ^4G$ + 14 $3d^8(^3F)4f\ ^2G$
520 375	520 467	−92	2.5	34 $3d^8(^3F)4f\ ^2D$ + 19 $3d^8(^3F)4f\ ^4F$ + 14 $3d^8(^3F)4f\ ^4P$
522 704	522 921	−217	1.5	35 $3d^8(^3F)4f\ ^4F$ + 29 $3d^8(^3F)4f\ ^2P$ + 12 $3d^8(^3P)5p\ ^2D$
522 873	522 988	−115	2.5	35 $3d^8(^3F)4f\ ^4P$ + 29 $3d^8(^3F)4f\ ^2F$ + 20 $3d^8(^3F)4f\ ^4D$
522 966	523 102	−136	1.5	22 $3d^8(^3F)4f\ ^4S$ + 24 $3d^8(^3P)5p\ ^2D$ + 16 $3d^8(^3F)4f\ ^2D$
523 286	523 334	−48	2.5	31 $3d^8(^3F)4f\ ^4F$ + 30 $3d^8(^3F)4f\ ^2D$ + 27 $3d^8(^3F)4f\ ^4G$
523 286	523 400	−114	3.5	33 $3d^8(^3F)4f\ ^4G$ + 30 $3d^8(^3F)4f\ ^4H$ + 30 $3d^8(^3F)4f\ ^2F$
524 631	524 745	−114	0.5	42 $3d^8(^3F)4f\ ^2P$ + 24 $3d^8(^3F)4f\ ^2S$ + 18 $3d^8(^3F)4f\ ^4D$
525 335	525 222	113	1.5	53 $3d^8(^3F)4f\ ^2D$ + 21 $3d^8(^3F)4f\ ^2P$ + 14 $3d^8(^3F)4f\ ^4F$
525 362	525 237	125	3.5	51 $3d^8(^3F)4f\ ^2G$ + 16 $3d^8(^3F)4f\ ^2F$ + 10 $3d^8(^3F)4f\ ^4H$
525 651	525 378	273	2.5	44 $3d^8(^3F)4f\ ^2F$ + 23 $3d^8(^3F)4f\ ^4G$ + 20 $3d^8(^3F)4f\ ^2D$
540 246	539 959	287	3.5	52 $3d^8(^1D)4f\ ^2G$ + 20 $3d^8(^1D)4f\ ^2F$ + 15 $3d^8(^3P)4f\ ^4F$
540 357	540 623	−266	1.5	69 $3d^8(^1D)4f\ ^2D$ + 16 $3d^8(^3P)4f\ ^4F$ + 8 $3d^8(^3P)4f\ ^2D$
540 517	540 748	−231	2.5	69 $3d^8(^1D)4f\ ^2F$ + 12 $3d^8(^3P)4f\ ^2F$ + 10 $3d^8(^3P)4f\ ^4F$
544 401	544 565	−164	2.5	77 $3d^8(^3P)4f\ ^4F$ + 10 $3d^8(^1D)4f\ ^2D$ + 9 $3d^8(^1D)4f\ ^2F$
544 950	545 011	−61	3.5	74 $3d^8(^3P)4f\ ^2F$ + 17 $3d^8(^1D)4f\ ^2G$
545 735	545 609	126	2.5	74 $3d^8(^3P)4f\ ^2F$ + 16 $3d^8(^1D)4f\ ^2F$ + 6 $3d^8(^1D)4f\ ^2D$
545 926	545 985	−59	3.5	70 $3d^8(^3P)4f\ ^4G$ + 20 $3d^8(^3P)4f\ ^2G$
546 268	546 291	−23	2.5	91 $3d^8(^3P)4f\ ^4G$
546 448	546 299	149	1.5	77 $3d^8(^3P)4f\ ^4D$ + 15 $3d^8(^1D)4f\ ^2P$
546 687	546 728	−41	3.5	74 $3d^8(^3P)4f\ ^4D$ + 11 $3d^8(^3P)4f\ ^2G$
546 801	546 852	−51	2.5	79 $3d^8(^3P)4f\ ^2D$ + 12 $3d^8(^3P)4f\ ^4D$
551 998	552 151	−153	1.5	99 $3d^8(^1G)4f\ ^2P$
552 156	552 217	−61	0.5	99 $3d^8(^1G)4f\ ^2P$
552 998	552 900	98	2.5	99 $3d^8(^1G)4f\ ^2D$
553 080	552 953	127	1.5	99 $3d^8(^1G)4f\ ^2D$
553 823	553 794	29	3.5	99 $3d^8(^1G)4f\ ^2F$
553 853	553 809	44	2.5	99 $3d^8(^1G)4f\ ^2F$
597 172	597 364	−192	3.5	86 $3d^8(^1S)4f\ ^2F$
597 358	597 320	38	2.5	97 $3d^8(^1S)4f\ ^2F$

Table 6. Same as Table 6 for Ga VI.

E_{exp} [a]	E_{calc} [b]	ΔE	J	Leading components (in %) in LS coupling[c]
				Even parity
0.0	23	−23	4	99 $3d^8\ ^3F$
3193.3	3187	7	3	100 $3d^8\ ^3F$
5164.0	5147	17	2	97 $3d^8\ ^3F$
20 531.6	20 507	24	2	75 $3d^8\ ^1D$ + 23 $3d^8\ ^3P$
25 683.2	25 765	−82	2	76 $3d^8\ ^3P$ + 23 $3d^8\ ^1D$
26 123.7	26 090	33	1	99 $3d^8\ ^3P$
26 607.4	26 583	24	0	99 $3d^8\ ^3P$
34 249.4	34 249	0	4	99 $3d^8\ ^1G$
78 106.2	78 106	0	0	99 $3d^8\ ^1S$
290 618.2	290 800	−182	5	99 $3d^7(^4F)4s\ ^5F$
292 766.3	292 860	−94	4	98 $3d^7(^4F)4s\ ^5F$
294 471.9	294 500	−28	3	99 $3d^7(^4F)4s\ ^5F$
295 691.7	295 677	15	2	99 $3d^7(^4F)4s\ ^5F$
296 472.6	296 434	39	1	99 $3d^7(^4F)4s\ ^5F$
301 417.4	301 448	−31	4	97 $3d^7(^4F)4s\ ^3F$
304 315.6	304 249	67	3	98 $3d^7(^4F)4s\ ^3F$
306 203.6	306 086	118	2	98 $3d^7(^4F)4s\ ^3F$
315 882.7	315 630	252	3	99 $3d^7(^4P)4s\ ^5P$
316 294.3	316 164	130	2	93 $3d^7(^4P)4s\ ^5P$ + 7 $3d^7(^2P)4s\ ^3P$
317 488.8	317 343	146	1	95 $3d^7(^4P)4s\ ^5P$
320 898.8	320 801	97	5	95 $3d^7(^2G)4s\ ^3G$
321 960.7	321 825	136	4	89 $3d^7(^2G)4s\ ^3G$ + 6 $3d^7(^2G)4s\ ^1G$
323 491.8	323 313	178	3	99 $3d^7(^2G)4s\ ^3G$
325 408.1	325 312	96	2	69 $3d^7(^4P)4s\ ^3P$ + 22 $3d^7(^2P)4s\ ^3P$

Notes. [a] From Shirai et al. (2007). [b] This work. [c] Only the first three components that are larger than 5% are given.

Table 6. continued.

E_{exp} [a]	E_{calc} [b]	ΔE	J	Leading components (in %) in LS coupling[c]
325 534.2	325 658	−124	1	61 $3d^7(^4P)4s\ ^3P$ + 17 $3d^7(^2P)4s\ ^1P$ + 16 $3d^7(^2P)4s\ ^3P$
326 334.7	326 610	−275	0	62 $3d^7(^4P)4s\ ^3P$ + 38 $3d^7(^2P)4s\ ^3P$
327 159.5	327 026	133	4	85 $3d^7(^2G)4s\ ^1G$ + 8 $3d^7(^2G)4s\ ^3G$ + 6 $3d^7(^2H)4s\ ^3H$
327 438.9	327 661	−222	2	54 $3d^7(^2P)4s\ ^3P$ + 29 $3d^7(^4P)4s\ ^3P$ + 8 $3d^7(^2D)4s\ ^3D$
328 609.6	328 863	−253	1	56 $3d^7(^2P)4s\ ^3P$ + 27 $3d^7(^4P)4s\ ^3P$ + 12 $3d^7(^2D)4s\ ^3D$
330 355.3	330 540	−185	6	100 $3d^7(^2H)4s\ ^3H$
330 724.3	330 909	−184	0	62 $3d^7(^2P)4s\ ^3P$ + 38 $3d^7(^4P)4s\ ^3P$
331 283.5	331 036	247	3	77 $3d^7(^2D)4s\ ^3D$ + 22 $3d^7(^2D)4s\ ^3D$
331 468.2	331 596	−127	5	92 $3d^7(^2H)4s\ ^3H$ + 5 $3d^7(^2H)4s\ ^1H$
331 810.7	332 168	−357	1	30 $3d^7(^2D)4s\ ^3D$ + 35 $3d^7(^2P)4s\ ^1P$ + 22 $3d^7(^2P)4s\ ^3P$
333 121.7	332 906	216	2	58 $3d^7(^2D)4s\ ^3D$ + 15 $3d^7(^2D)4s\ ^3D$ + 12 $3d^7(^2D)4s\ ^1D$
333 146.0	333 197	−51	4	89 $3d^7(^2H)4s\ ^3H$ + 9 $3d^7(^2G)4s\ ^1G$
336 722.0	336 845	−123	5	93 $3d^7(^2H)4s\ ^1H$
336 737.8	336 877	−139	1	47 $3d^7(^2P)4s\ ^1P$ + 36 $3d^7(^2D)4s\ ^3D$ + 8 $3d^7(^2D)4s\ ^3D$
338 579.5	338 262	317	2	64 $3d^7(^2D)4s\ ^1D$ + 16 $3d^7(^2D)4s\ ^1D$ + 9 $3d^7(^2D)4s\ ^3D$
353 118.1	353 017	101	2	99 $3d^7(^2F)4s\ ^3F$
353 484.3	353 445	39	3	98 $3d^7(^2F)4s\ ^3F$
354 120.4	354 202	−81	4	99 $3d^7(^2F)4s\ ^3F$
359 164.4	358 908	256	3	98 $3d^7(^2F)4s\ ^1F$
386 276.8	386 420	−143	1	81 $3d^7(^2D)4s\ ^3D$ + 18 $3d^7(^2D)4s\ ^3D$
386 736.8	386 856	−119	2	79 $3d^7(^2D)4s\ ^3D$ + 19 $3d^7(^2D)4s\ ^3D$
387 630.8	387 680	−49	3	77 $3d^7(^2D)4s\ ^3D$ + 22 $3d^7(^2D)4s\ ^3D$
392 566.6	392 381	185	2	77 $3d^7(^2D)4s\ ^1D$ + 20 $3d^7(^2D)4s\ ^1D$
				Odd parity
389 525.6	389 705	−179	4	46 $3d^7(^4F)4p\ ^5F$ + 43 $3d^7(^4F)4p\ ^5D$
389 982.7	390 077	−94	5	83 $3d^7(^4F)4p\ ^5F$ + 12 $3d^7(^4F)4p\ ^5G$
391 766.2	391 842	−76	3	64 $3d^7(^4F)4p\ ^5F$ + 26 $3d^7(^4F)4p\ ^5D$
393 500.8	393 554	−53	4	40 $3d^7(^4F)4p\ ^5D$ + 31 $3d^7(^4F)4p\ ^5F$ + 20 $3d^7(^4F)4p\ ^5G$
393 529.7	393 535	−6	2	77 $3d^7(^4F)4p\ ^5F$ + 15 $3d^7(^4F)4p\ ^5D$
394 800.7	394 760	41	1	90 $3d^7(^4F)4p\ ^5F$ + 6 $3d^7(^4F)4p\ ^5D$
395 468.8	395 363	105	6	99 $3d^7(^4F)4p\ ^5G$
395 680.0	395 697	−17	3	46 $3d^7(^4F)4p\ ^5D$ + 32 $3d^7(^4F)4p\ ^5G$ + 12 $3d^7(^4F)4p\ ^5F$
395 852.3	395 778	74	5	64 $3d^7(^4F)4p\ ^5G$ + 19 $3d^7(^4F)4p\ ^3G$ + 16 $3d^7(^4F)4p\ ^5F$
397 051.5	396 903	148	4	62 $3d^7(^4F)4p\ ^5G$ + 20 $3d^7(^4F)4p\ ^5F$ + 7 $3d^7(^4F)4p\ ^3G$
397 186.4	397 110	76	2	57 $3d^7(^4F)4p\ ^5G$ + 33 $3d^7(^4F)4p\ ^5D$ + 5 $3d^7(^4P)4p\ ^5D$
397 796.8	397 630	167	3	55 $3d^7(^4F)4p\ ^5G$ + 21 $3d^7(^4F)4p\ ^5F$ + 15 $3d^7(^4F)4p\ ^5D$
398 136.8	398 032	105	2	38 $3d^7(^4F)4p\ ^5D$ + 34 $3d^7(^4F)4p\ ^5G$ + 18 $3d^7(^4F)4p\ ^5F$
398 298.7	398 456	−157	1	77 $3d^7(^4F)4p\ ^5D$ + 14 $3d^7(^4P)4p\ ^5D$ + 6 $3d^7(^4F)4p\ ^5F$
398 323.3	398 808	−484	0	83 $3d^7(^4F)4p\ ^5D$ + 16 $3d^7(^4P)4p\ ^5D$
400 532.9	400 594	−61	5	75 $3d^7(^4F)4p\ ^3G$ + 24 $3d^7(^4F)4p\ ^5G$
401 119.8	401 287	−167	4	85 $3d^7(^4F)4p\ ^3F$
403 397.9	403 573	−175	3	76 $3d^7(^4F)4p\ ^3F$ + 11 $3d^7(^4F)4p\ ^3D$
403 630.9	403 670	−39	4	86 $3d^7(^4F)4p\ ^3G$ + 12 $3d^7(^4F)4p\ ^5G$
405 118.4	405 325	−207	3	74 $3d^7(^4F)4p\ ^3D$ + 10 $3d^7(^4F)4p\ ^3F$ + 6 $3d^7(^4F)4p\ ^3G$
405 283.3	405 368	−85	2	82 $3d^7(^4F)4p\ ^3F$ + 5 $3d^7(^2G)4p\ ^3F$ + 5 $3d^7(^4F)4p\ ^3D$
405 788.3	405 819	−31	3	87 $3d^7(^4F)4p\ ^3G$
406 689.7	406 268	422	2	94 $3d^7(^4P)4p\ ^5S$
406 843.7	407 034	−190	2	80 $3d^7(^4F)4p\ ^3D$
408 054.2	408 232	−178	1	86 $3d^7(^4F)4p\ ^3D$
418 007.1	418 354	−347	1	20 $3d^7(^4P)4p\ ^3S$ + 23 $3d^7(^2P)4p\ ^3P$ + 23 $3d^7(^4P)4p\ ^5D$
419 168.0	418 962	206	2	64 $3d^7(^4P)4p\ ^5D$ + 12 $3d^7(^4F)4p\ ^5D$ + 5 $3d^7(^2P)4p\ ^3D$
419 588.7	419 233	355	3	68 $3d^7(^4P)4p\ ^5D$ + 11 $3d^7(^4P)4p\ ^3D$ + 10 $3d^7(^4F)4p\ ^5D$
419 644.6	419 860	−215	0	71 $3d^7(^4P)4p\ ^5D$ + 16 $3d^7(^4F)4p\ ^5D$ + 12 $3d^7(^2P)4p\ ^3P$
419 928.7	419 635	294	5	60 $3d^7(^2G)4p\ ^3H$ + 19 $3d^7(^2G)4p\ ^1H$ + 13 $3d^7(^2G)4p\ ^3G$
420 030.7	419 914	117	4	53 $3d^7(^2G)4p\ ^3F$ + 12 $3d^7(^2G)4p\ ^3G$ + 7 $3d^7(^2G)4p\ ^1G$
420 527.4	420 388	140	1	51 $3d^7(^4P)4p\ ^5D$ + 20 $3d^7(^4P)4p\ ^3S$ + 8 $3d^7(^4F)4p\ ^5D$
421 348.9	420 967	382	4	78 $3d^7(^4P)4p\ ^5D$ + 9 $3d^7(^2G)4p\ ^3H$ + 7 $3d^7(^4F)4p\ ^5D$
421 619.2	421 269	350	4	73 $3d^7(^2G)4p\ ^3H$ + 6 $3d^7(^4P)4p\ ^5D$ + 6 $3d^7(^2G)4p\ ^1G$
422 597.0	422 985	−388	0	64 $3d^7(^2P)4p\ ^3P$ + 15 $3d^7(^2D)4p\ ^3P$ + 9 $3d^7(^4P)4p\ ^5D$
4228 86.4	423 582	−695	2	51 $3d^7(^2P)4p\ ^3P$ + 10 $3d^7(^2D)4p\ ^3P$ + 8 $3d^7(^2D)4p\ ^3D$
422 914.6	422 580	334	6	92 $3d^7(^2G)4p\ ^3H$ + 5 $3d^7(^2H)4p\ ^3I$
423 585.8	423 481	105	3	58 $3d^7(^2G)4p\ ^3F$ + 26 $3d^7(^2G)4p\ ^3G$
423 703.8	424 083	−379	1	39 $3d^7(^2P)4p\ ^3P$ + 20 $3d^7(^4P)4p\ ^5P$ + 15 $3d^7(^4P)4p\ ^3S$

Table 6. continued.

E_{exp} [a]	E_{calc} [b]	ΔE	J	Leading components (in %) in LS coupling[c]
424 443.2	424 617	−174	2	38 $3d^7(^4P)4p\ ^5P$ + 19 $3d^7(^2P)4p\ ^3D$ + 14 $3d^7(^2P)4p\ ^1D$
424 594.2	424 682	−88	4	41 $3d^7(^2G)4p\ ^1G$ + 27 $3d^7(^2G)4p\ ^3F$ + 16 $3d^7(^2H)4p\ ^1G$
425 094.4	424 778	316	3	45 $3d^7(^4P)4p\ ^5P$ + 25 $3d^7(^4P)4p\ ^3D$ + 12 $3d^7(^4P)4p\ ^5D$
425 555.0	425 598	−43	5	78 $3d^7(^2G)4p\ ^3G$ + 13 $3d^7(^2G)4p\ ^1H$
425 605.8	425 489	116	3	41 $3d^7(^2G)4p\ ^1F$ + 13 $3d^7(^2G)4p\ ^3F$ + 9 $3d^7(^2D)4p\ ^1F$
425 879.8	425 655	225	2	25 $3d^7(^4P)4p\ ^3D$ + 32 $3d^7(^4P)4p\ ^5P$ + 12 $3d^7(^4P)4p\ ^5D$
426 209.2	425 945	264	1	55 $3d^7(^4P)4p\ ^5P$ + 31 $3d^7(^4P)4p\ ^3S$
426 636.8	426 393	244	3	45 $3d^7(^4P)4p\ ^3D$ + 28 $3d^7(^4P)4p\ ^5P$ + 11 $3d^7(^2G)4p\ ^3G$
426 905.5	426 737	168	2	91 $3d^7(^2G)4p\ ^3F$ + 5 $3d^7(^4F)4p\ ^3F$
426 973.4	427 112	−138	1	47 $3d^7(^4P)4p\ ^3D$ + 31 $3d^7(^2P)4p\ ^3D$ + 6 $3d^7(^4P)4p\ ^5D$
427 106.4	426 883	224	5	51 $3d^7(^2G)4p\ ^1H$ + 25 $3d^7(^2G)4p\ ^3H$ + 15 $3d^7(^2H)4p\ ^3G$
427 165.0	427 256	−91	4	68 $3d^7(^2G)4p\ ^3G$ + 11 $3d^7(^2G)4p\ ^3H$ + 10 $3d^7(^2G)4p\ ^1G$
427 399.6	427 489	−89	5	75 $3d^7(^2H)4p\ ^3G$ + 8 $3d^7(^2G)4p\ ^3H$ + 8 $3d^7(^2G)4p\ ^1H$
427 521.7	427 595	−73	3	48 $3d^7(^2G)4p\ ^3G$ + 15 $3d^7(^2G)4p\ ^1F$ + 14 $3d^7(^2G)4p\ ^3F$
428 109.0	428 450	−341	0	55 $3d^7(^2P)4p\ ^1S$ + 32 $3d^7(^4P)4p\ ^3P$ + 7 $3d^7(^2P)4p\ ^3P$
428 511.4	428 539	−28	6	62 $3d^7(^2H)4p\ ^3I$ + 32 $3d^7(^2H)4p\ ^1I$
428 900.4	428 718	182	2	41 $3d^7(^4P)4p\ ^3P$ + 20 $3d^7(^4P)4p\ ^3D$ + 13 $3d^7(^2D)4p\ ^3P$
429 939.8	429 858	82	3	53 $3d^7(^2D)4p\ ^3D$ + 16 $3d^7(^2D)4p\ ^3D$ + 11 $3d^7(^2P)4p\ ^3D$
430 034.0	429 946	88	1	29 $3d^7(^4P)4p\ ^3P$ + 23 $3d^7(^2P)4p\ ^3D$ + 18 $3d^7(^4P)4p\ ^3D$
430 045.3	430 064	−19	4	83 $3d^7(^2H)4p\ ^3G$ + 7 $3d^7(^2F)4p\ ^3G$
430 311.9	430 215	97	5	87 $3d^7(^2H)4p\ ^3I$ + 7 $3d^7(^2G)4p\ ^1H$
430 599.5	430 430	169	2	34 $3d^7(^4P)4p\ ^3P$ + 24 $3d^7(^4P)4p\ ^3D$
430 763.4	430 639	124	3	45 $3d^7(^2P)4p\ ^3D$ + 29 $3d^7(^2D)4p\ ^3F$ + 9 $3d^7(^4P)4p\ ^5P$
431 050.7	431 069	−18	7	100 $3d^7(^2H)4p\ ^3I$
431 443.0	431 231	212	2	35 $3d^7(^2D)4p\ ^3D$ + 14 $3d^7(^2P)4p\ ^3P$ + 8 $3d^7(^2D)4p\ ^3F$
431 472.8	431 286	186	1	31 $3d^7(^2D)4p\ ^3D$ + 32 $3d^7(^4P)4p\ ^3P$ + 11 $3d^7(^2P)4p\ ^1P$
432 400.5	432 318	82	3	70 $3d^7(^2H)4p\ ^3G$ + 8 $3d^7(^2F)4p\ ^3G$ + 5 $3d^7(^2D)4p\ ^1F$
432 409.2	432 363	46	1	27 $3d^7(^2P)4p\ ^3D$ + 24 $3d^7(^4P)4p\ ^3P$ + 17 $3d^7(^4P)4p\ ^3D$
432 884.7	433 322	−437	2	51 $3d^7(^2P)4p\ ^3D$ + 17 $3d^7(^2P)4p\ ^1D$ + 14 $3d^7(^2D)4p\ ^3F$
434 590.0	435 071	−481	0	59 $3d^7(^4P)4p\ ^3P$ + 39 $3d^7(^2P)4p\ ^1S$
434 789.2	434 451	338	4	77 $3d^7(^2D)4p\ ^3F$ + 19 $3d^7(^2D)4p\ ^3F$
434 837.6	434 868	−31	6	64 $3d^7(^2H)4p\ ^1I$ + 31 $3d^7(^2H)4p\ ^3I$
435 668.5	435 429	240	3	34 $3d^7(^2D)4p\ ^3F$ + 18 $3d^7(^2P)4p\ ^3D$ + 12 $3d^7(^2G)4p\ ^1F$
436 426.1	436 287	139	2	32 $3d^7(^2D)4p\ ^3F$ + 16 $3d^7(^2D)4p\ ^3D$ + 14 $3d^7(^2D)4p\ ^1D$
436 778.4	437 476	−697	1	41 $3d^7(^2P)4p\ ^3S$ + 22 $3d^7(^2P)4p\ ^1P$ + 13 $3d^7(^2D)4p\ ^3P$
437 611.7	437 792	−180	1	31 $3d^7(^2P)4p\ ^1P$ + 32 $3d^7(^2P)4p\ ^3S$ + 10 $3d^7(^2D)4p\ ^1P$
437 682.7	437 402	281	2	30 $3d^7(^2P)4p\ ^1D$ + 24 $3d^7(^2D)4p\ ^1D$ + 19 $3d^7(^2D)4p\ ^3P$
438 288.5	438 502	−214	6	95 $3d^7(^2H)4p\ ^3H$
438 999.3	439 151	−152	5	90 $3d^7(^2H)4p\ ^3H$
440 038.2	440 138	−100	4	93 $3d^7(^2H)4p\ ^3H$
440 844.9	440 591	254	2	35 $3d^7(^2D)4p\ ^3P$ + 17 $3d^7(^2D)4p\ ^1D$ + 13 $3d^7(^2P)4p\ ^3P$
441 145.2	441 087	58	4	64 $3d^7(^2H)4p\ ^1G$ + 32 $3d^7(^2G)4p\ ^1G$
442 214.5	441 897	317	3	54 $3d^7(^2D)4p\ ^1F$ + 15 $3d^7(^2G)4p\ ^1F$ + 11 $3d^7(^2D)4p\ ^1F$
443 348.5	443 266	82	1	28 $3d^7(^2D)4p\ ^3P$ + 28 $3d^7(^2D)4p\ ^1P$ + 18 $3d^7(^2P)4p\ ^1P$
444 362.8	444 087	276	1	47 $3d^7(^2D)4p\ ^1P$ + 22 $3d^7(^2D)4p\ ^3P$ + 10 $3d^7(^2P)4p\ ^3S$
444 367.4	444 172	195	0	67 $3d^7(^2D)4p\ ^3P$ + 15 $3d^7(^2P)4p\ ^3P$ + 10 $3d^7(^2D)4p\ ^3P$
445 925.7	446 115	−189	5	92 $3d^7(^2H)4p\ ^1H$
453 517.0	453 556	−39	2	48 $3d^7(^2F)4p\ ^1D$ + 37 $3d^7(^2F)4p\ ^3F$ + 6 $3d^7(^2F)4p\ ^3D$
454 836.1	454 763	73	3	66 $3d^7(^2F)4p\ ^3G$ + 18 $3d^7(^2F)4p\ ^3F$ + 9 $3d^7(^2H)4p\ ^3G$
455 557.5	455 595	−37	4	48 $3d^7(^2F)4p\ ^3G$ + 25 $3d^7(^2F)4p\ ^3F$ + 17 $3d^7(^2F)4p\ ^1G$
456 583.9	456 632	−48	3	56 $3d^7(^2F)4p\ ^3D$ + 22 $3d^7(^2F)4p\ ^3F$ + 6 $3d^7(^2F)4p\ ^3G$
457 762.6	457 892	−129	2	53 $3d^7(^2F)4p\ ^3F$ + 27 $3d^7(^2F)4p\ ^1D$ + 12 $3d^7(^2F)4p\ ^3D$
458 164.9	458 229	−64	3	52 $3d^7(^2F)4p\ ^3F$ + 26 $3d^7(^2F)4p\ ^3D$ + 13 $3d^7(^2F)4p\ ^3G$
458 730.8	458 800	−69	2	69 $3d^7(^2F)4p\ ^3D$ + 18 $3d^7(^2F)4p\ ^1D$
458 909.2	458 844	65	1	88 $3d^7(^2F)4p\ ^3D$ + 6 $3d^7(^2D)4p\ ^3D$
459 016.3	458 967	49	4	33 $3d^7(^2F)4p\ ^1G$ + 40 $3d^7(^2F)4p\ ^3G$ + 22 $3d^7(^2F)4p\ ^3F$
459 106.5	459 152	−45	5	92 $3d^7(^2F)4p\ ^3G$ + 7 $3d^7(^2H)4p\ ^3G$
459 534.9	459 658	−123	4	47 $3d^7(^2F)4p\ ^3F$ + 46 $3d^7(^2F)4p\ ^1G$
466 715.5	466 703	12	3	93 $3d^7(^2F)4p\ ^1F$
483 570.3	483 606	−36	2	76 $3d^7(^2D)4p\ ^3P$ + 20 $3d^7(^2D)4p\ ^3P$
484 260.9	484 370	−109	1	78 $3d^7(^2D)4p\ ^3P$ + 16 $3d^7(^2D)4p\ ^3P$
485 120.7	485 225	−104	0	83 $3d^7(^2D)4p\ ^3P$ + 15 $3d^7(^2D)4p\ ^3P$
486 095.0	486 101	−6	2	75 $3d^7(^2D)4p\ ^3F$ + 17 $3d^7(^2D)4p\ ^3F$
487 831.8	487 778	53	3	70 $3d^7(^2D)4p\ ^3F$ + 18 $3d^7(^2D)4p\ ^3F$

Table 6. continued.

E_{exp} [a]	E_{calc} [b]	ΔE	J	Leading components (in %) in LS coupling[c]
490 450.6	490 439	12	4	74 $3d^7(^2D)4p\ ^3F$ + 21 $3d^7(^2D)4p\ ^3F$
492 658.4	492 654	4	1	73 $3d^7(^2D)4p\ ^1P$ + 10 $3d^7(^2D)4p\ ^1P$ + 7 $3d^7(^2D)4p\ ^3D$
493 464.9	493 300	164	3	71 $3d^7(^2D)4p\ ^1F$ + 18 $3d^7(^2D)4p\ ^1F$ + 5 $3d^7(^2D)4p\ ^3F$
497 330.1	497 361	−31	1	67 $3d^7(^2D)4p\ ^3D$ + 20 $3d^7(^2D)4p\ ^3D$ + 9 $3d^7(^2D)4p\ ^1P$
497 893.6	497 965	−72	2	65 $3d^7(^2D)4p\ ^3D$ + 20 $3d^7(^2D)4p\ ^3D$ + 8 $3d^7(^2D)4p\ ^1D$
498 920.8	499 062	−141	2	61 $3d^7(^2D)4p\ ^1D$ + 22 $3d^7(^2D)4p\ ^1D$ + 7 $3d^7(^2D)4p\ ^3D$
499 867.4	499 869	−1	3	68 $3d^7(^2D)4p\ ^3D$ + 24 $3d^7(^2D)4p\ ^3D$

Table 11. Statistics of the model atoms used in our calculations for G191−B2B.

Ion		Levels NLTE	Levels LTE	Lines	Ion		Levels NLTE	Levels LTE	Super lines	Sample lines
H	I	14	2	91	Fe	III	7	0	25	537 689
	II	1	–	–		IV	7	0	25	3 102 371
He	I	45	0	121		V	7	0	25	3 266 247
	II	16	16	120		VI	8	0	33	991 935
	III	1	–	–		VII	9	0	39	200 455
C	II	1	45	0		VIII	1	0	0	
	III	58	9	329	Ni	III	7	0	22	1 033 920
	IV	54	4	295		IV	7	0	25	2 512 561
	V	1	0	0		V	7	0	27	2 766 664
N	II	15	232	18		VI	7	0	27	7 407 763
	III	34	32	129		VII	8	0	33	4 195 381
	IV	90	4	546		VIII	1	0	0	
	V	54	8	297	IG	III	1	0	0	
	VI	1	0	0		IV	7	0	25	1 581 144
O	II	1	46	0		V	7	0	23	2 230 921
	III	72	0	322		VI	7	0	25	1 455 521
	IV	38	56	173		VII	7	0	24	1 129 512
	V	76	50	472		VIII	1	0	0	
	VI	54	8	291	Zn	III	1	0	0	
	VII	1	0	0		IV	7	0	11	400
Al	II	1	4	0		V	7	0	15	1 879
	III	7	29	10		VI	1	0	0	
	IV	6	183	3	Ga	III	1	0	0	
	V	6	223	4		IV	7	0	19	3 198
	VI	1	0	0		V	7	0	15	517
Si	III	17	17	28		VI	7	0	13	1 914
	IV	16	7	44		VII	1	0	0	
	V	1	0	0	Ge	IV	1	0	0	
P	III	3	7	0		V	7	0	16	2 159
	IV	21	30	9		VI	7	0	12	414
	V	18	7	12		VII	1	0	0	
	VI	1	0	0	Ba	IV	1	0	0	
S	III	1	230	0		V	7	0	12	981
	IV	17	83	32		VI	7	0	6	162
	V	39	71	107		VII	7	0	11	493
	VI	25	12	48		VIII	1	0	0	
	VII	1	0	0						
Sn	III	3	18	2						
	IV	6	4	1						
	V	5	4	0						
	VI	6	0	0						
	VII	1	0	0						
				total	17	78	1013	1441	4012	32 424 201

Notes. IG is a generic model atom that comprises Ca, Sc, V, Ti, Cr, Mn, and Co. The NLTE levels for elements with an atomic number >20 are super levels build from the individual atomic levels, and the super lines include the sample lines (Kurucz LIN lines, cf. Rauch & Deetjen 2003).

Table 12. Same as Table 11, for RE 0503−289.

Ion		Levels NLTE	Levels LTE	Lines	Ion		Levels NLTE	Levels LTE	Super lines	Sample lines
He	I	74	29	69	Fe	III	7	0	25	537 689
	II	16	16	120		IV	7	0	25	3 102 371
	III	1	–	–		V	7	0	25	3 266 247
C	III	16	117	30		VI	8	0	33	991 935
	IV	54	4	295		VII	1	0	0	0
	V	0	1	0	Ni	III	7	0	22	1 033 920
N	III	18	48	42		IV	7	0	25	2 512 561
	IV	48	46	201		V	7	0	27	2 766 664
	V	35	27	149		VI	7	0	27	7 407 763
	VI	0	1	0		VII	1	0	0	0
O	III	1	1	0	IG	III	7	0	24	4 963 441
	IV	69	28	432		IV	7	0	25	1 581 144
	V	90	44	610		V	7	0	23	2 230 921
	VI	14	48	33		VI	7	0	25	1 455 521
	VIII	0	1	0		VII	1	0	0	0
Si	III	1	33	0	Zn	III	1	0	0	0
	IV	16	7	44		IV	7	0	11	400
	V	1	0	0		V	7	0	15	1 879
P	IV	1	50	0		VI	1	0	0	0
	V	18	7	12	Ga	III	1	0	0	0
	VI	1	0	0		IV	7	0	19	3 198
S	IV	1	99	0		V	7	0	15	517
	V	23	87	47		VI	7	0	13	1 914
	VI	12	25	25		VII	1	0	0	0
	VII	1	1	0	Ge	IV	1	0	0	0
						V	7	0	16	2 159
						VI	7	0	12	414
						VII	1	0	0	0
					Kr	III	1	25	0	0
						IV	38	0	0	0
						V	25	0	0	0
						VI	46	0	887	0
						VII	14	0	37	0
						VIII	1	0	0	0
					Xe	III	11	11	0	0
						IV	44	0	0	0
						V	29	0	0	0
						VI	82	0	887	0
						VII	86	3	2	0
						VIII	1	0	0	0
					Ba	IV	1	0	0	0
						V	7	0	12	981
						VI	7	0	6	162
						VII	7	0	11	493
						VIII	1	0	0	0
				total	16	70	953	870	4358	31 862 294

Table 15. Strongest Ga lines in the stellar-atmosphere models of RE 0503−289.

Wavelength/Å	Ion	W_λ/mÅ	Id	Comment
953.738	Ga VI	0.97	–	
965.237 965.272	Ga IV	2.23	:	blend
979.383	Ga VI	0.99	–	
979.614	Ga V	3.65	:	
980.240	Ga VI	1.07	:	
980.988	Ga V	2.88	–	
981.831	Ga IV	1.57	:	
984.078	Ga V	3.09	:	
1002.985	Ga VI	1.49	:	
1004.170	Ga VI	1.15	–	blend Ba V λ 1004.093 Å
1006.396	Ga VI	2.55	–	
1006.894	Ga VI	1.54	:	
1008.924	Ga VI	2.44	:	
1009.512	Ga VI	1.03	:	
1009.928	Ga V	6.07	+	
1010.102	Ga VI	1.88	:	
1011.047	Ga VI	2.29	:	
1014.434 1014.456	Ga VI Ga V	12.34	:	blend Xe VI λ 1014.505 Å
1014.868	Ga V	2.19	:	blend O IV λ 1014.90 Å
1015.598 1015.610	Ga VI Ga V	6.19	+	blend
1019.711	Ga V	8.30	+	
1032.375	Ga V	2.51	–	
1033.549	Ga V	3.83	:	
1034.822	Ga V	1.15	–	blend Xe VI λ 1034.784 Å
1038.778	Ga V	5.12	:	
1040.204	Ga V	1.79	:	
1045.850	Ga V	3.36	:	
1047.504	Ga V	5.08	:	blend O IV λ 1047.590 Å
1050.453	Ga V	16.83	+	blend O IV λ 1050.505 Å
1054.430	Ga V	1.70	–	
1054.563	Ga V	5.07	:	blend Ge V λ 1054.590 Å
1058.123	Ga V	14.02	+	blend Zn V λ 1058.190 Å
1062.677	Ga V	10.84	+	blend Ge V λ 1062.574 Å
1063.807	Ga V	3.61	:	
1065.371	Ga V	1.34	–	
1066.724	Ga V	8.25	:	blend Si IV $\lambda\lambda$ 1066.636, 1066.650 Å
1068.593 1068.616	Ga V	7.90	+	blend
1069.484 1069.530 1069.587	Ga V	15.77	:	blend
1071.123 1071.168	Ga V	11.28	+	blend
1073.791 1073.814	Ga V Ga VI	11.12	+	blend
1074.911 1074.966	Ga V Ga IV	1.12	:	blend
1078.225	Ga V	2.31	:	
1079.587 1079.599	Ga V	11.47	+	blend
1080.474	Ga V	1.84	:	
1080.988	Ga V	3.72	:	blend Xe VI λ 1080.869 Å
1087.358	Ga V	2.64	–	blend (unknown)
1088.068	Ga V	1.27	–	
1091.703	Ga V	9.56	+	blend Xe VI λ 1091.634 Å
1094.355	Ga V	11.50	+	
1094.739	Ga V	3.16	–	blend Se V λ 1094.68 Å
1095.110	Ga V	11.66	:	blend
1100.401	Ga V	7.83	:	
1101.613	Ga V	9.68	+	
1102.767 1102.803	Ga V	20.30	+	blend
1103.047	Ga V	12.37	:	
1104.936	Ga V	8.42	+	
1105.253	Ga V	2.33	–	
1105.620	Ga V	8.47	+	
1107.763	Ga V	0.86	–	blend C IV $\lambda\lambda$ 1107.591.1107.930, 1107.979 Å
1109.829	Ga V	1.45	–	
1115.561	Ga V	9.91	+	

Notes. The given wavelengths correspond to those given in Tables 7–9. Column 3 gives the equivalent widths of the computed lines. Column 4 denotes "−" = not observed, "+" = observed, ":" = uncertain.

Table 15. continued.

Wavelength/Å	Ion	W_λ/mÅ	Id	Comment
1118.018	Ga V	1.23	–	blend P V λ 1117.976 Å
1118.318	Ga V	10.79	:	
1120.260	Ga V	2.80	–	blend Zn V λ 1120.325 Å
1123.154	Ga V	11.90	+	
1123.646	Ga V	10.79	:	blend (unknown)
1126.393	Ga V	17.59	+	blend (two Ga V lines, same λ)
1127.332	Ga V	2.42	:	
1127.726 1127.752	Ga V	20.80	+	blend
1128.082	Ga V	13.16	:	blend P V λ 1128.000 Å
1128.554	Ga V	14.86	+	blend S V $\lambda\lambda$ 1128.666, 1128.779 Å
1129.956	Ga V	12.35	+	
1131.452	Ga V	10.79	:	blend (unknown)
1132.054	Ga V	4.38	–	
1132.157	Ga V	3.04	–	
1133.247	Ga V	4.08	–	
1133.903	Ga V	3.99	:	
1136.067	Ga V	12.35	+	
1138.187	Ga V	7.88	:	blend Zn V λ 1138.248 Å
1143.367	Ga V	3.02	:	blend Zn V $\lambda\lambda$ 1143.304, 1143.403 Å
1145.974	Ga V	2.05	–	
1148.409	Ga V	3.65	:	
1150.113	Ga V	3.31	+	
1150.219	Ga V	16.35	+	
1155.976	Ga V	2.19	–	
1156.190	Ga IV	1.94	–	blend Zn V λ 1156.394 Å
1156.511	Ga V	13.04	+	blend Zn V λ 1156.520 Å
1157.729	Ga V	2.43	:	
1158.534	Ga V	3.83	–	blend Zn V λ 1158.476 Å
1160.847	Ga V	1.28	:	
1163.609	Ga IV	1.77	–	
1170.585	Ga IV	3.32	:	
1178.795	Ga V	4.22	:	blend Zn V λ 1078.808 Å
1183.110	Ga V	1.45	–	blend Zn V λ 1183.024 Å
1183.656	Ga V	3.00	–	
1185.226	Ga IV	2.00	–	